ELECTROMAGNETIC SHIELDING OF A BUILDING: MODELING AND MEASUREMENT

by

Piraye Karacagil

B.S. in E.E, İstanbul Technical University, 1993

Submitted to the Institute for Graduate Studies in Science and Engineering in partial fulfillment of the requirements for the degree of Master of Science in Electrical and Electronic Engineering

Boğaziçi University

1997

ACKNOWLEDGMENTS

I would sincerely like to thank all who have helped me during this study. First of all, I would like to thank my thesis supervisor Prof. Dr. Selim ŞEKER for his help to select this topic by giving the necessary motivation at the initial steps and wonderful guidance during each and every stage of this work.

I acknowledge the facilities provided by TUBITAK MAM UEKAE EMC Lab. and I would like to thank the staff for their contributions during the measurements. I am particularly grateful to Dr. Temel YALÇIN, Fatih ÜSTÜNER, İbrahim ÖLÇER, Selçuk HELHEL and Ebru KÖKSALDI for their helpful comments.

This study is dedicated to my parents. Without their loving help and encouragement, nothing would be possible.

ABSTRACT

In this thesis, shielding effectiveness of a building is calculated by using a multilayer model and compared with the results of the measurements taken inside a building.

The computer program used for this objective has been constructed to simulate the importance of the multilayer structures. For the same and different floors in a building, shielding effectiveness values are calculated and compared with the experimental results. Measured values are obtained by using an automated measuring system developed for this study. Furthermore, the shielding effectiveness measurements of the shielded enclosures (Gigahertz Transverse Electromagnetic (GTEM) and Compact Diagnostis Chamber (CDC)) in accordance with the MIL-STD 285 and IEEE 299 are also carried out as another experimental study of this thesis.

All results obtained for different frequency ranges and at different places are presented with several graphics.

BİNANIN ELEKTROMANYETİK EKRANLAMASI: MODELLEME VE ÖLÇMELER

ÖZET

Bu tezde binaların ekranlama etkinliği çok katmanlı model kullanılarak hesaplanıp bina içinde yapılan ölçmelerden elde edilen sonuçlarla mukayese edilmiştir.

Bu amaç doğrultusunda kullanılan bilgisayar programı çok katmanlı yapıların önemini ortaya koyacak şekilde tasarlanmıştır. Bina içindeki aynı ve farklı katlardaki ekranlama etkinliği bu programla hesaplanıp deneysel sonuçlarla karşılaştırılır. Ölçme değerleri bu çalışmada geliştirilen otomatik ölçme sistemi kullanılarak elde edilmiştir. Ayrıca ekranlı odaların (GTEM ve CDC) MIL-STD 285 ve IEEE 299 standartlarına uygun olarak ekranlama etkinliklerinin ölçülmesi de, bu tezde deneysel çalışma olarak gerçekleştirilmiştir.

Farklı frekans bölgelerinde ve değişik yerlerde yapılan ölçmelerin sonuçları grafikler halinde sunulmuştur.

TABLE OF CONTENTS

Page

LIST OF FIGURES

Page

LIST OF TABLES

Page

1. INTRODUCTION

Quantitative data on the attenuation of electromagnetic fields by building structures is useful in a number of engineering applications. Because of the potential implementation of indoor wireless local area networks (LAN's) and personal communication networks (PCN's) it is important to understand the propagation of signals inside buildings.

Electromagnetic shielding properties of houses or buildings are usually determined by measuring the signals generated by either portable equipment or by fixed equipment present in the vicinity. Smith [1] presented the results of an empirical investigation of the shielding properties of seven buildings ranging from a single family of detached residences to multistory office buildings. Both electric and magnetic field attenuation were measured in the frequency range of about 20 kHz to 500 MHz. On site measurements are time consuming and expensive. One method to overcome this difficulty is to use a computer code , which calculates the attenuation of buildings as a function of its material characteristics, dimension, room layout , frequency and the incidence angle of radiation.

Indoor propagation study is more complex than outdoor. The environment inside a building consists of many obstructions, constructed from different materials, and these objects may be in close distance to the transmitter and receiver antennas of the measurement system during experiments. The indoor environments are not uniform in comparison to outdoor environment. The space and height between furniture, architectural configurations, partition materials and even moving people can fluctuate the radio signals. Thus, the intensity of the radio signals varies from place to place within a building.

Because of the presence of these varying conditions, some approximation should be made for modeling of buildings. From the earlier studies in the literature, one may conclude that the approximations made in those research can be classified into two main groups: In the first one, several measurements are made and then a formula is searched for modeling the measured data. The attenuation characteristics of the building is now approximated by the formula. Lafortune and Lecours [2] examined the effects of the number of walls, number of floors, open and closed doors, corridors, windows between antennas.

In the other method, modeling takes the precedence: according to the architecture of the building a prediction formula is firstly proposed to estimate the attenuation

characteristics of buildings. Then measurements are carried out to verify the assumed model.

This thesis studies the shielding properties of buildings, which are here, modeled as multilayer structures. Some previous unpublished studies about multilayer modeling have been used to investigate the effects of the Nuclear Electromagnetic Pulse (NEMP) [3] and the effects of different incident angles of radiation on the multilayer structures[4]. Rooms housed through a corridor form a multilayer structure. On the other hand floors can also be assumed as a multilayer. Because of these similarities, this multilayer model has been used in our study. Propagation losses inside buildings are investigated by this approximation. Multilayer modeling enables us to obtain transmission and reflection coefficients of the layers, which are actually the rooms and/or floors that we are interested in.

Honcharenko, Bertoni, Diling [5],[6] studied on propagation losses of the same and different floors inside a building. The research reported here contributes to their study by repeating the measurements to verify the above mentioned multilayer model, and also not at a single frequency but for a range of frequencies. The propagation loss measurements have been carried out in two steps: in the first step, both the transmitting and the receiving antenna have been located on the same floor and the frequency range of 200 MHz-1000 MHz has been used; where in the second step, the receiver has been moved one floor down and measurements have been repeated at the single frequency of 980 MHz. Measured data were obtained by using an automated measurement system which provides a synchronization between signal generator and receiver. As the number of floors and/or rooms between the transmitter and the receiver is increased, depending on the structure of the building and the location of the antennas, the propagation characteristics and the signal sector average will be determined by either the direct ray propagation through floors or diffraction outside the building for both directed and diffracted rays. Calculated results of the propagation losses are compared with the measured ones for the same and different floors. The building of the electronics department at TÜBİTAK Marmara Research Center was selected as the measurement site and measurements were carried out for both electric and magnetic field components.

Chapter 2 reviews the basics of the electromagnetic shielding theory. Description of the shielding effectiveness is given in this part and loss components are described. Properties of different kinds shielding were also discussed in this section.

Chapter 3 deals with the importance of shielding applications in buildings and typical building attenuation is presented here.

Multilayer model is introduced in Chapter 4. Basic theory of this model is described and the sudy of Honcharenko, Bertoni, Diling [5],[6] are presented in which this model to be substituted.

The experimental part of the thesis is covered in Chapter 5. Test facilities, TÜBİTAK MRC Electronic department are presented and automated test system used for obtaining the measured data is discussed in this chapter. Results for both measured and calculated data are compared also in this part.

Additional experimental study concerning the shielding effectiveness measurements of shielded enclosures, GTEM and Compact Diagnostic Chamber, and the measurement procedures MIL-Std 285 and IEEE 299 are presented in Chapter 6 as a case study.

Chapter 7 includes comments on the research done and suggestions for future study.

2. SHIELDING THEORY

2.1. Introduction

Shielding is a major category of Electromagnetic Interference (EMI) control at all levels of Electromagnetic Compatibility (EMC), viz., component; chassis or black box; equipment; subsystem; system; and entire vehicular or housing structures, such as ships, aircraft, and buildings. This section presents shielding theory, shielding materials, and some mathematical models of shielding effectiveness.

The performance of shielding is a function of whether the source appears as an electric or magnetic field in the near-in induction region or an electromagnetic field in the far field region. These considerations are a function of both the source and receptor geometry separation, and frequency of operation. Consequently, it is pertinent to first establish criteria for far and near-fields as a function of these parameters.

2.2. Electromagnetic Field Theory

The purpose of this section is to present some pragmatic relations about magnetic, electric and electromagnetic fields as pertinent background to understanding and applying shielding criteria. Since the literature is exist with excellent discussions of Maxwell's equations and field theory, only a few aspects are presented here.

The electric (E_θ, E_r) and magnetic (H_ϕ) fields (Fig. 2.1) existing about an oscillating doublet are obtained from applying Maxwell's equations [7]:

$$E_\theta = Z_0 k \sin\theta \left[-\left(\frac{\lambda}{2\pi r}\right)^2 \cos\left(\frac{2\pi r}{\lambda} - wt\right) - \frac{\lambda}{2\pi r}\sin\left(\frac{2\pi r}{\lambda} - wt\right) + \cos\left(\frac{2\pi r}{\lambda} - wt\right)\right] \quad (2.1)$$

$$E_r = -2Z_0 k \cos\theta \left[\left(\frac{\lambda}{2\pi r}\right)\cos\left(\frac{2\pi}{\lambda} - wt\right) + \frac{\lambda}{2\pi r}\sin\left(\frac{2\pi}{\lambda} - wt\right)\right] \quad (2.2)$$

$$H_\phi = k \sin\theta \left[\frac{\lambda}{2\pi r} \sin\left(\frac{2\pi r}{\lambda} - wt \right) + \cos\left(\frac{2\pi r}{\lambda} - wt \right) \right] \tag{2.3}$$

where,

$k = ID/2r\lambda$

θ = zenith angle to radial distance r

I = current in short wire of length D ($D \ll \lambda$)

$\omega = 2\pi f$ (radial frequency)

λ = wavelength corresponding to frequency, $f = c/\lambda$

r = distance from wire to measuring or observation point

t = time= 1/f

Z_0 = free-space impedance ($r \gg \lambda/2\pi$)

$= E_\theta/H_\phi = \sqrt{\mu_0/\varepsilon_0} = 120\pi = 377\Omega$

$c = 1/\sqrt{\mu_0/\varepsilon_0} = 3 \times 10^8$ m/s

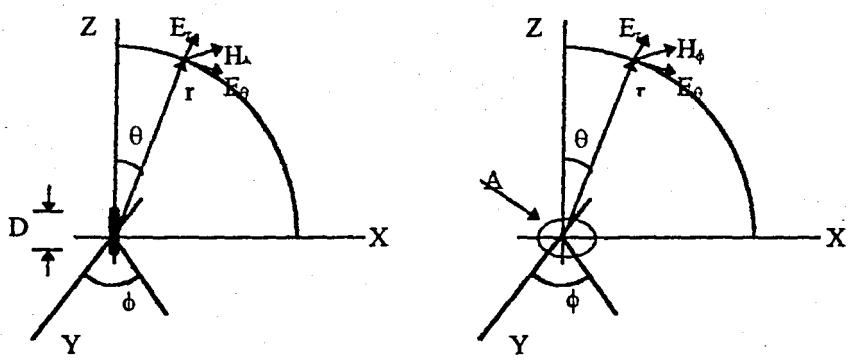

Figure. 2.1. Spherical Coordinates Used in Eqs. 2.1-2.3

Several observation can be made out about the near and far fields from Eqs. (2.1) and (2.3). (E_r is dropped from further discussion because it represents a nonpropagating component of the E field.):

(1) The multiplier k, contains a 1/r component which also decreases with distance from the source.

(2) When multiplier, $\lambda/2\pi r$, equals 1 in two of the three E_θ electric field terms and the magnetic field term, all coefficients of either the sin or cos are unity an equal. Thus,

when $r=\lambda/2\pi$ (about one-sixth wavelength), this corresponds to the transition field condition or boundary between the near-field (first term of both equations) and far-field (last term).

(3) When $r>>\lambda/2\pi$ (far-field conditions), only the last term of each equation is significant. For this condition the wave impedance $Z_0=E_\theta/H_\phi=377$ohms. This is called the radiation field (plane waves) and both E_θ and the H_ϕ are in time phase although in directional quadrature.

(4) When $r<<\lambda/2\pi$ (near-field conditions), only the first term of each equation is significant. For this condition, the wave impedance, $E_\theta/H_\phi=Z_0\ \lambda/2\pi r$. Note that the wave impedance is now $Z_w>>Z_0$ since $\lambda/2\pi r>>1$. This sometimes called simply an electric-field or a high-impedance field, i.e., high relative to a plane wave impedance. It is also the induction field and E_θ and H_ϕ are in both the phase and directional quadrature.

(5) Had the oscillating source not been a small straight wire or doublet exhibiting high circuit impedance but rather a small wire loop of Area A (Fig.2.1),exhibiting low impedance, the first term appearing in Eq (2.1) would vanish and a similar first term would appear in Eq. (2.3). For this condition, the wave impedance in the near field. $E_\theta/H_\phi=Z_0 2\pi r/\lambda$. Note that the wave impedance is now $Z_w<<Z_0$ for $\lambda/2\pi r>>1$. This is sometimes called magnetic field or low-impedance field, i.e., low relative to Z_0 the plane wave (radiation) impedance.

Figure 2.2 illustrate the first four of the above observations for amplitude of each of the electric-field terms in Eq.(2.1). Note that the quasi-stationary field is the largest term in the far field and the induction is next largest; whereas the radiation term is largest in the far field.

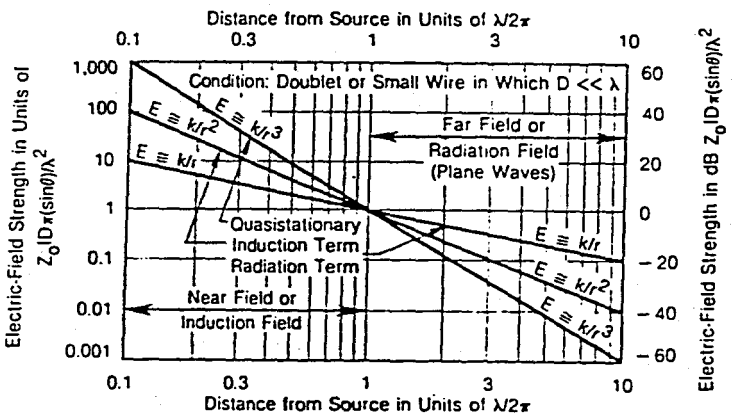

Figure 2.2. Electric-Field Strength vs. Source Distance [7]

For r=λ/2π, the coefficient of all three terms are equal Figure 2.3 illustrate the preceding 4th and 5th observations in the near or induction field. Figure 2.3a shows a short monopole or straight wire in which the circuit current is low. Consequently the source or circuit impedance= V/I is a high impedance. As previously shown, the wave impedance close to the source is also high, relative to 377 Ω. The associated electric field attenuates more rapidly ($1/r^3$) with an increase in distance than the magnetic field ($1/r^2$) in the induction region. Thus the wave impedance decreases linearly (20 dB per decade)with an increase in distance where it asymptotically approaches Z_0=377 Ω in the far or radiation field for r>>λ/2π. This relation is depicted in Fig.2.4.

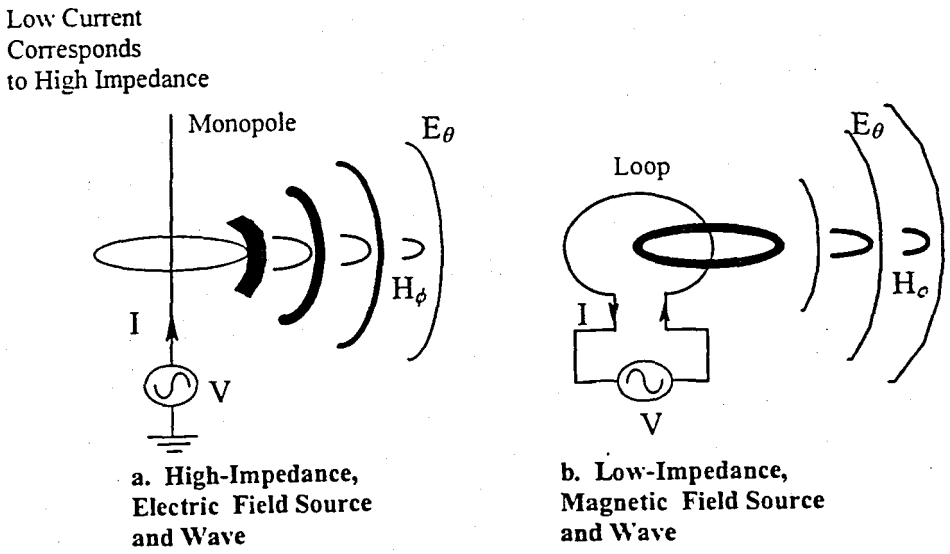

Figure 2.3. Conceptual Illustration of Field Strengths vs. Source Type and Distance

The converse to the above applies for Fig.2.3b. where in low impedance radiation source creates a low-impedance wave, i.e., a magnetic field. This wave impedance increases linearly (20 dB per decade) with distance where it asymptotically approaches 377Ω in the far field. Fig 2.4. is also illustrates this wave impedance as a function of distance, r.

When the dimension D of an emission source (e.g., a wire or an antenna) becomes an appreciable fraction of a wavelength, the expressions presented in Eqs. (2.1) to (2.3) no longer apply. Different relations must then be used since the curvature of the arriving wave front no longer permits the incremental elements of an antenna or radiating source to be in phase.

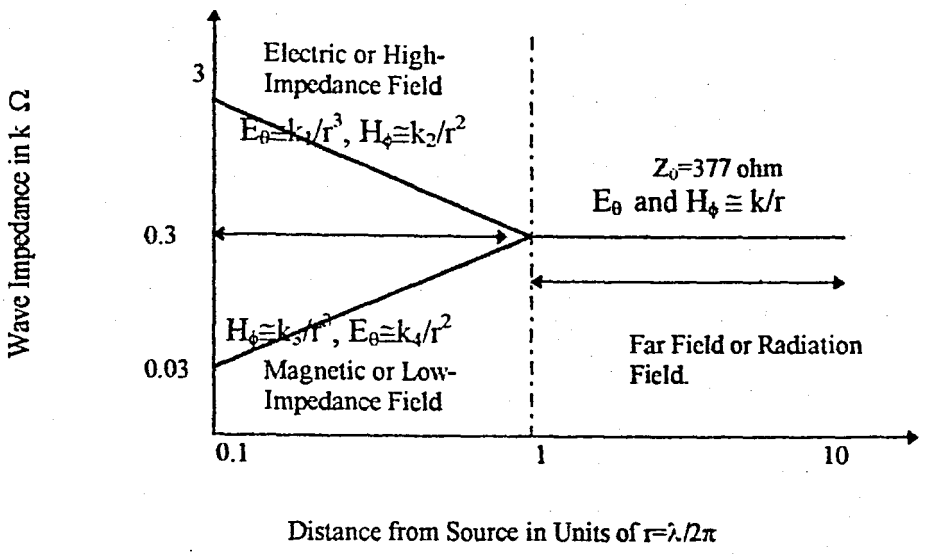

Figure 2.4. Wave Impedance as a Function of Source Distance

2.3. Wave Impedance

Electromagnetic wave impedance is a function of the impedance of source circuit generating the wave and the frequency. Summing up, the wave impedance, Z_w is:

$$Z_w = E/H = kZ_0 = k\sqrt{\mu/\varepsilon} = 120\pi k = k377\Omega \tag{2.4}$$

provided that the length of the source emission-generating circuit element is D << λ.

where,

$k \approx \frac{\lambda}{2\pi r}$ for current source (very high impedance) and r≤ λ/2π (2.5)

$k \approx \frac{2\pi r}{\lambda}$ for voltage source (very low impedance) and r≤ λ/2π (2.6)

$k \approx 1$ for any network impedance and r≥λ/2π (2.7)

2.4. Metal Impedance

All homogenous materials are characterized by a quantity known as the intrinsic impedance of the material Z_i:

$$Z_i = \sqrt{\frac{jw\mu}{\sigma + jw\varepsilon}} \tag{2.8}$$

For air conductivity is extremely small $\sigma << \omega\varepsilon$ thus the intrinsic impedance Eq. (2.8) for air becomes:

$$Z_a = \sqrt{\frac{\mu}{\varepsilon}} = \sqrt{\frac{\mu_0}{\varepsilon_0}} = 120\pi = 377\Omega \tag{2.9}$$

2.4.1. Barrier Impedance of Metals

In contrast to air and low-loss dielectrics, metals are defined as materials whose conductivity is extremely high relative to air such that $\sigma >> \varpi\varepsilon$. Thus the intrinsic impedance of Eq. (2.8) for a metal becomes:

$$Z_m = \sqrt{\frac{jw\mu}{\sigma}} = \sqrt{\frac{j2\pi f\mu}{\sigma}} = (1+j)\sqrt{\frac{\pi f\mu}{\sigma}} \tag{2.10}$$

Surface impedance is based on metal thickness which is very much greater than the skin depth, $t >> \delta$. ($\delta = 1/\sqrt{\sigma\pi f\mu} = \sqrt{2}/\sigma Z_m$) As the frequency approach zero, $\delta \to \infty$, and $Z_m \to 0$

For the metals that he thickness of the barrier is less than the skin depth $t < 3\delta$. In this case barrier impedance is independent form the permeability of the materials and the frequency.[8]

$$Z_B = \frac{Z_m}{(1-e^{-t/\delta})} \qquad (Z_B=Z_m \text{ for } t/\delta>>1) \tag{2.11}$$

$$Z_B = \delta Z_m / t = \frac{\sqrt{2}}{\sigma t} \qquad (t/\delta<<1) \tag{2.12}$$

2.5. Shielding Effectiveness

Shielding provided by a metallic barrier can be analyzed from either of two viewpoints: (1) that of field or wave theory or (2) that of circuit theory. In the circuit-theory approach, currents from the interference source induced currents in the shield such that the associated external fields due to both currents are out of phase and tend to cancel. Since the field theory approach is more widely adopted in the literature, however it will be used in the remainder of this discussion.

A shield is, conceptually a barrier to the transmission of the electromagnetic fields. For low frequencies the effectiveness of magnetic shields can be calculated using a quasi-static theory in which the determining factor is the reluctance of the path followed by lines of magnetic flux. At higher frequencies for nonmagnetic material transmission line model is used in which skin depth model plays a major role.

Shielding effectiveness is defined as Eq.(2.13):

$$SE_{dB} = 10\log\left(\frac{incident\ \ power\ \ density}{transmitted\ \ power\ \ density}\right) \tag{2.13}$$

where,

incident power density.= power density at measuring point
before shield is in place

transmitted power density = power density at same measuring point
after shield is in place.

Equation (2.13) is defined as a loss so that the SE is always positive. Since power density in W/m^2 can also be expressed as the product of E(V/m) multiplied by H(A/m), SE can be written as:[8]

$$SE_{dB} = 10\log\frac{E_b H_b}{E_a H_a} \tag{2.14}$$

where,

E_b, H_b = Value of E and H fields before shielding

E_a, H_a = Value of E and H fields after shielding

If the wave impedance Z_w =E/H is the same before and after i.e. if the attenuation of the barrier is identical for the E and the H terms, or if the emerging field is measured at a far field distance from the shield in stable field conditions:

$$H_b = \frac{E_b}{Z_w} \tag{2.15}$$

$$H_a = \frac{E_a}{Z_w} \tag{2.16}$$

therefore,

$$SE_{dB} = 10\log\frac{E_b^2 / Z_w}{E_a^2 / Z_w} = 10\log\frac{E_b^2}{E_a^2} = 20\log\frac{E_b}{E_a} \tag{2.17}$$

In stabilized field conditions, therefore the measure of SE in power density terms or in field terms gives the same results.

In terms of the field strength, Eq. (2.18) may also be defined as follows as long as the two fields are measured in the same medium having the same wave impedance: [8]

$$SE_{dB} = 20\log\left(\frac{E_b}{E_a}\right) \qquad \text{for electric fields} \tag{2.18}$$

$$SE_{dB} = 20\log\left(\frac{H_b}{H_a}\right) \qquad \text{for magnetic fields} \tag{2.19}$$

where

E_b= electric field strength before shield is installed

E_a= electric field strength after shield is installed

H_b= magnetic field strength before shield is installed

H_a= magnetic field strength after shield is installed

Equations (2.18) and (2.19) give identical results in the far field ($r>>\lambda/2\pi$) but do not result in the same SE_{dB} in the near field since the wave impedances are different.

Figure 2.5 depicts the phenomena of both reflection and transmission that are utilized in removing energy from an incident wave (plane wave example shown). If an incident plane wave is intercepted by a barrier to its passage, at the region A of the interface, both reflection and transmission occur. The amplitudes of these two portions of the original wave depend on the surface impedance of the barrier material with respect to the impedance of the wave. Since the reflected wave is not proceeding in a direction that contributes to the surviving wave on the far side of the barrier, this is considered a loss mechanism.

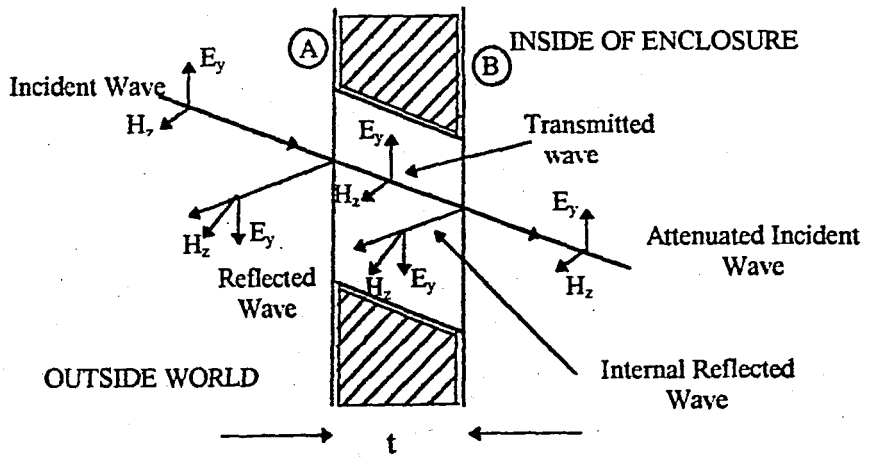

Figure 2.5 Representation of Shielding Phenomena for Plane Waves

The transmitted portion of the incident wave, continuing on in approximately the same direction after penetrating the interface, experiences absorption while traversing the finite thickness of the barrier. At the second barrier interface B of Fig. 2.5. reflection and transmission phenomena again occur. The transmitted portion is the amount of energy that transversed the first interface less the energy absorbed in transversing the barrier and that

reflected at B. The second reflection contributes an insignificant amount in the removal of energy and is usually neglected.

At plane wave (far-field) frequencies, the shielding effectiveness of a barrier in reducing the energy of a barrier in reducing the energy of an electromagnetic field can be readily computed. Each of the contributing factors discussed above is computed separately and then their total contribution is summarized. This is accomplished in the following manner for expressing shielding effectiveness in dB,

$$SE_{dB} = R_{dB} + A_{dB} + B_{dB} \tag{2.20}$$

where,

R_{dB}= reflection loss in dB

A_{dB}= transmission or absorption loss in dB

B_{dB}= internal reflection loss at exiting interface in dB (usually neglected)

2.5.1. Absorption Loss

The absorption loss, A_{dB} is independent of the type of wave impinging on the shield and is expressed as follows[7]:

$$A_{dB} = 131.4x10^{-3} t\sqrt{f\sigma_r\mu_r} = 131.4t\sqrt{f_{MHz}\sigma_r\mu_r}.dB \tag{2.21}$$

where,

A= attenuation in dB

t=.thickness of barrier in mm

f= frequency in Hz

f_{MHz}= frequency in MHz

σ_r = conductivity, relative to copper (σ for Cu=1)

μ_r =. magnetic permeability of material relative to vacuum or copper (μ=1)

Eq. (2.21) is plotted in Fig 2.6 for the parameters copper (σ_r =1, μ_r =1), iron (σ_r = 0.17, μ_r=1000), and hypernick (σ_r=0.06, μ_r=80,000) Absorbtion loss is the dependent

variable and frequency is the independent variable with thickness in mm as a second parameter. It is noted that the brute-source approach of using a thick sheet of iron at low frequencies (e.g., at 60 Hz) results in a significant absorption loss (approx. 45 dB). On the other hand a thin shield of copper at 1 GHz yields significant (>100 dB) absorption loss. This illustrates the difficulty of achieving a significant absorption loss at ELF in contrast to UHF.

The internal reflection loss, B, in Eq. 2.20 is negligible when A_{dB} is greater than about 4dB. When A_{dB} is not greater than 4dB, B_{dB} is negative since it is coherent term which would have made E_a in Eq.2.18 larger. The value of B_{dB} is shown in the lower right corner of Fig.2.6

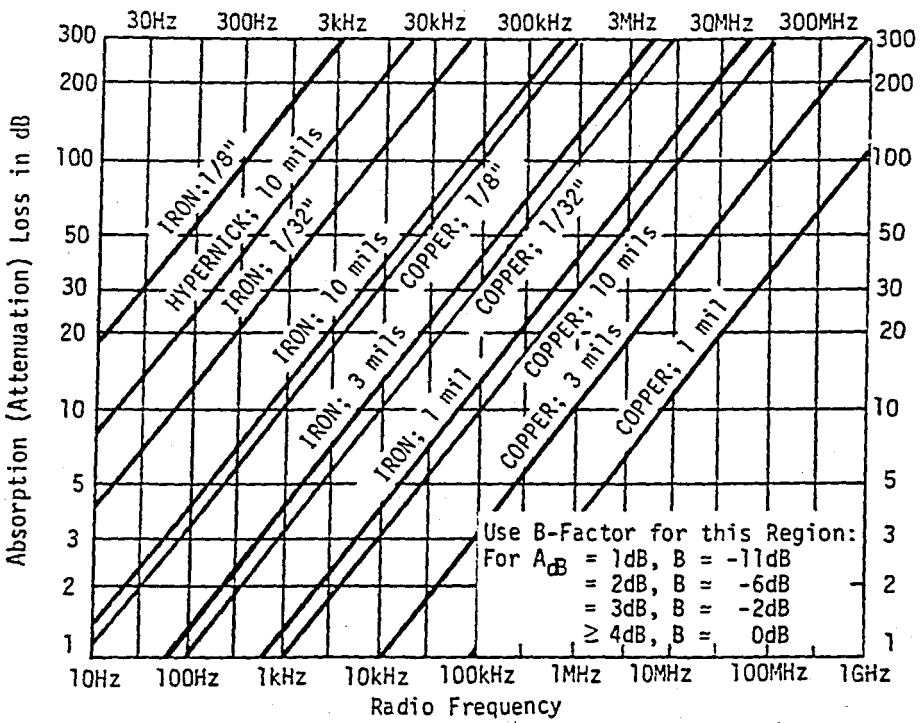

Figure 2.6 Shielding Absorption loss vs. Radio Freq., Material, and Thickness[7]

2.5.2. Reflection Loss.

Reflection loss, R_{dB}, is represented by forming the ratio of the wave impedance, Z_w to surface impedance of barrier material Z_b. [7]

$$R_{dB} = 20\log_{10}\frac{(K+1)^2}{4K} \approx 20\log_{10}\left(\frac{Z_w}{4Z_b}\right), \qquad \text{for K>10} \tag{2.22}$$

Eq. (2.22) indicates that if either the wave impedance is high (e.g. electric field) and/or the barrier surface impedance is low (e.g. copper), the loss will be substantial. Conversely if the wave impedance is. low (e.g. magnetic field) and/or the barrier impedance is relatively high (e.g. iron), the reflection loss will be significantly less. Each of this situations is now discussed in further detail.

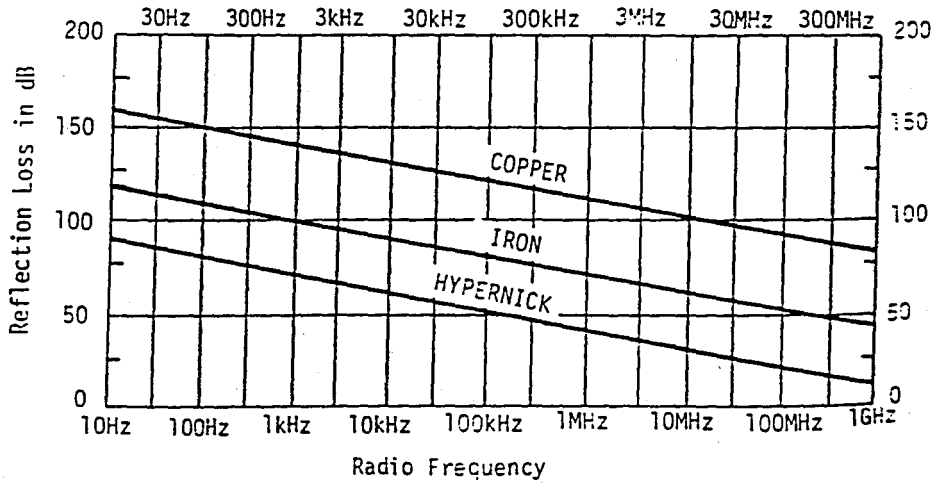

Fig 2.7 Reflection of loss of plane waves [7]

2.5.3. Reflection Loss to Plane Waves.

The reflection loss of a plane wave, R_{dB}, may also be calculated from: [7]

$$R_{dB} = 108 + 10\log_{10}^{(G/\mu f_{MHz})}\, dB \qquad (2.23)$$

Eq. (2.23) is plotted in Fig 2.7 for copper, iron and hypernick. Compared with absorption loss, the figure indicates that the reflection loss of plane waves at low frequencies is the major attenuation mechanism. High conductivity, low permeability material is more effective in establishing reflection loss, since the barrier surface impedance is lower with regard to that of a plane wave where Z_w=377 ohms and the ratio of the latter to the former (the loss mechanism) is greater (cf. Eq.(2.22)). At UHF the reflection loss becomes less effective since the barrier skin depth decreases (surface resistivity increases) and the barrier impedance increases resulting in a smaller ratio of plane wave to barrier impedance. In comparing Figs (2.6) and (2.7), note that the absorption loss becomes more significant loss mechanism of the two.

2.5.4. Reflection Loss to Electric and Magnetic Fields

When there is substantial difference in the impedance of the incident wave and the shielding barrier, reflection at the boundary is significant and good shielding is obtained. The high impedance wave in the near field is known as an electric-field wave, and its reflection loss is: [7]

$$R_{dB} = 354 + 10\log_{10}^{\left(\frac{G}{f^3\mu r^2}\right)}\, dB \qquad (2.24)$$

where,

r = distance from source to barrier in inches the other terms are as defined under Eq. (2.21)

Eq. (2.24) is plotted in Fig. 2.8 for parameters of separation distances, r, of 1 inch, 1m and 30m; and for copper iron materials. As before, frequency is independent variable and the reflection loss, R_{dB}, is the dependent variable.

For low impedance or magnetic field waves, the reflection loss is [7]:

$$R_{dB} = 20\log_{10}^{\left[(0.462/r)\sqrt{\mu/fG}+0.136r\sqrt{Gf/\mu}+0.354\right]} dB \qquad (2.25)$$

Eq. 2.25 is plotted in Fig.2.9 for the parameters of separation distance, r, of 1 inch, 1m and 30m and for copper and iron materials. This reflection loss to iron approaches 0 dB at about 30 kHz, when the magnetic field wave impedance approximates that that of the barrier impedance (loss=0 dB from Eq. (2.22)). Below 30 kHz, the wave impedance is less than the barrier impedance and the loss again increases. The reflection loss of a magnetic field shown in the figure increases with frequency until the source to barrier separation distance is about $\lambda/2\pi$, whence the plane-wave losses of Fig. 2.7 again prevail.

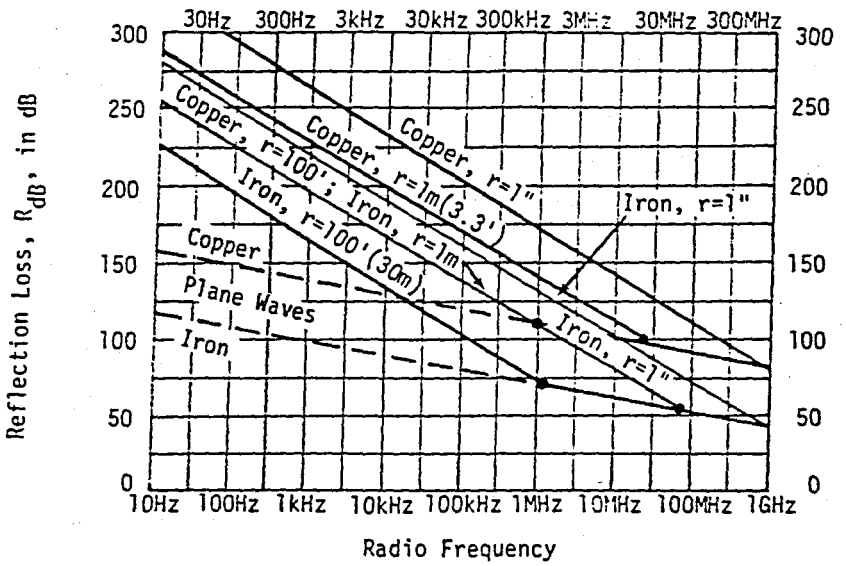

Figure 2.8 Reflection loss of Electric Fields vs. Radio Freq. [7]

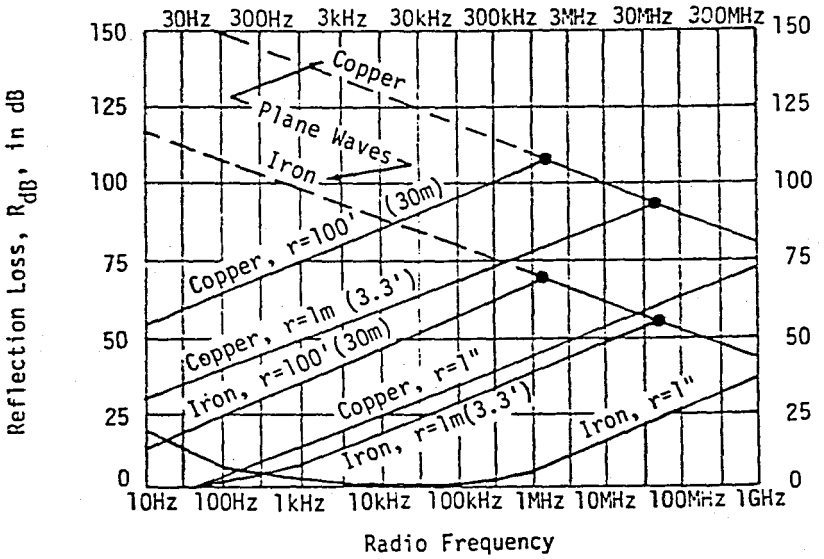

Figure 2.9 Reflection Loss of Magnetic Fields vs. Radio Freq. [7]

In comparing Figs. 2.8 and 2.9, it is noted that reflection to magnetic field at low frequencies is distinctly different from that for electric fields. Magnetic fields are shielded at DC and ELF only by providing a low reluctance path as an alternative for the incident magnetic field.

Fig. 2.10 depicts a simple representation of a uniform magnetic field existing in free space. The vertical lines show the direction of the orientation of the magnetic field vector throughout the two dimensions. Fig 2.11 shows the effect on the field lines by including a hollow permeable object in this uniform magnetic field. The field intensity lines enter the object at an angle of 90^0 to its surface. In the interior of this hollow object the field intensity lines are less intense than in the surrounding free space medium. However the magnetic field lines in the solid barrier are much more than in either the hollow center or the exterior of the barrier. This effect is due to the relative higher reluctances of free space both surrounding the barrier and the interior vs that of the barrier itself. The lower reluctances of the barrier divides the field intensity lines reducing the intensity of the absolute magnetic field in the interior of the enclosure to yield a shielding effect. This effect is quite pronounced at DC where shielding effectiveness values in excess of 50 dB have been

achieved through the utilization of extremely high permeability materials configured on a double barrier enclosure.

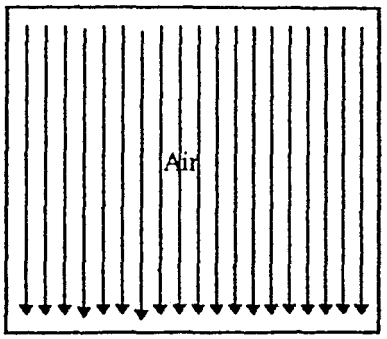

Figure 2.10. Uniform magnetic Field

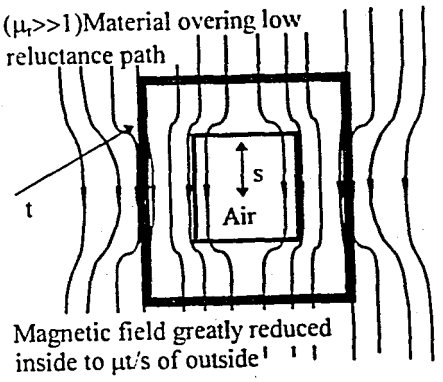

Figure 2.11 Cross Section of a Hollow Rectangular Solid of High Permeab.in Uniform Field

2.5.5. Composite Absorption and Reflection Loss

When either Eqs. 2.20 to 2.25 or Figs. 2.5 to 2.9 are combined, the over all attenuation or shielding effectiveness given in Eq. 2.18 results. These relationships are plotted in Fig. 2.12. Since there are vary variables, the composite curves represent the parameters of copper and iron materials having a thickness of one mil and 1/32 inch; electric and magnetic field and plane wave sources; and a source to barrier distance of 1 inch and 1 meter. Except for LF magnetic fields, the figure shows that reflection loss in the main mechanism at HF. Fig 2.12 is one of a family of mathematical models which defines shielding attenuation. Other curves show the effects of different materials, thickness and emission source distances.

2.6. Shielding Materials

This section summarizes the properties of homogeneous metals, pseudo-homogenous metals and small aperture metals.

2.6.1. Homogeneous Metals

Many of the metals and their associated conductivities and permeabilities which the designer might expect to encounter are listed in Table 2.1. The fourth column, entitled product $\sqrt{\sigma_r \mu_r}$ is a ranking of the latent absorbtion loss of metals relative to copper. For nonmagnetic materials, except silver, all σ_r , μ_r values relative to copper are less than 1.0. Thus non magnetic materials provide less absorption loss than copper.

All magnetic materials, on the other hand, have relative absorption loss values exceeding two and are relatively good absorbers of energy at low frequencies compared to nonmagnetic materials. On the other hand, since the relative permeability degrades with frequency, magnetic materials offer absorption losses less than nonmagnetic materials at higher frequencies (above approximately 100 kHz).

For thin-metal thicknesses (thicknesses for which $t/\delta << 1$) the metal absorption loss is negligible and the choise of metal, whether magnetic or nonmagnetic, for shielding effectiveness (SE) based on absorption loss is unimportant. However, when the metal is not thin (when t/δ is not $<<1$) the absorption loss becomes significant. Apart from cost and other considerations, columns 2 and 3 are useful in choosing a metal for shielding or extracting the applicable σ_r and μ_r values.

The fifth column of Table 2.1. [9] entitled Quotient $\sqrt{\sigma_r / \mu_r}$ is a ranking of the latent reflection loss of metals relative to copper. Expressed in dB form in column six, the nonmagnetic materials outperform nearly all magnetic materials for reflection loss performance. For thin metal thickness (thickness for $t/\delta << 1$) the reflection loss is the only important term for overall SE. For this condition then the designer would select a non-magnetic material of higher conductivity.

Table 2.1. Relative Conductivity and Permeability of Metals [9]

(1) Metal	(2) Rel. Conduct σ_r	(3) Rel. Perme $\mu_r \leq 10$ KHz)	(4) Prod $A=k\sqrt{\sigma_r \mu_r}$	(5) Quotient $R=k\sqrt{\sigma_r / \mu_r}$	(6) Rel.Ref lR_{dB}
1. Silver	1.064	1	1.03	1.3	+0.3
2. Copper (Solid)	1.00	1	1	1	0
3. Copper(Flame Spray)	0.10	1	0.32	0.32	-10.0
4. Gold	0.70	1	0.88	0.88	-1.1
5. Chromium	0.664	1	0.81	0.81	-1.8
6. Aluminum (Soft)	0.63	1	0.78	0.78	-2.1
7. Aluminum (Tempered)	0.40	1	0.63	0.63	-4.0
8. Aluminum (Household Foil , 1 mil)	0.53	1	0.73	0.73	-2.8
9. Aluminum (Household Foil ,1 mil)	0.61	1	0.78	0.78	-2.1
10. Aluminum (Flame Spray)	0.036	1	0.19	0.19	-14.4
11. Brass (91% Cu, 9% Zn)	0.47	1	0.69	0.69	-3.3
12. Brass (66% Cu, 34% Zn)	0.35	1	0.52	0.52	-5.7
13. Magnesium	0.38	1	0.61	0.61	-4.3
14. Zinc	0.305	1	0.57	0.57	-4.9
15. Tungsten	0.314	1	0.56	0.56	-5.0
16. Beryllium	0.33	1	0.53	0.53	-5.5
17. Cadmium	0.232	1	0.48	0.48	-6.3
18. Platinum	0.17	1	0.42	0.42	-7.6
19. Tin	0.151	1	0.39	0.39	-8.2
20. Tantalum	0.12	1	0.33	0.33	-9.6
21. Lead	0.079	1	0.28	0.28	-11.0
22. Monel (67 Ni ,30 Cu,2 Fe,1 Mn)	0.041	1	0.20	0.20	-13.9
23. Magnesene	0.039	1	0.20	0.20	-14.1
24. Titanium	0.036	1	0.19	0.19	-14.4
25. Mercury (Liquid)	0.018	1	0.13	0.134	-17.4
26. Nichrome (65 Ni,12 Cr,23 Fe)	0.0012	1	0.035	0.035	-29.2
27. Supermalloy	0.023	100,000	53.7	0.0005	-65.4
28. 78 Permalloy	0.108	8,000	29.4	0.0037	-48.7

29. Purified Iron	0.17	5,000	29.2	0.0058	-44.7
30. Conetic AA	0.031	20,000	28.7	0.0011	-58.8
31. 4-79 Permalloy	0.0314	20,000	25.1	0.0013	-58.0
32. Mumetal	0.0289	20,000	24.0	0.0012	-58.4
33. Permendur (50 Cu,1-2V,& Fe)	0.247	800	14.1	0.018	-35.1
34. Hypernick	0.0345	4,500	12.5	0.0028	-51.1
35. 45 Permalloy (1200 Anneal)	0.0384	4,000	12.4	0.0031	-50.2
36. 45 Permalloy (1050 Anneal)	0.0384	2,500	9.80	0.0039	-48.1
37. Hot-Rolled Silicon Steel	0.0384	1,500	7.59	0.0051	-45.9
38. Sinimax	0.0192	3,000	7.59	0.0025	-51.9
39. 4% Silicon Iron (Grain Oriented)	0.037	1,500	7.45	0.0050	-46.1
40. 4% Silicon Iron	0.029	500	3.81	0.0076	-42.4
41. 16 Alfenol	0.0113	4,500	7.13	0.0016	-56.0
42. Hiperco	0.069	650	6.70	0.010	-39.7
43. Monimax	0.0216	2,000	6.57	0.0033	-49.7
44. 50% Nickel Iron	0.0384	1,000	6.20	0.0062	-44.2
45. 45-25 Perminvar	0.091	400	6.03	0.015	-36.4
46. Commercial Iron (0.2% Impure)	0.17	200	5.83	0.29	-30.7
47. Cold-Rolled Steel	0.17	180	5.53	0.031	-30.2
48. Nickel	0.23	100	4.70	0.047	-26.6
49. Stainless Steel (1Cu, 18Cr, 8Ni, & Fe)	0.02	200	2.00	0.010	-40.0
50. Rhometal (36 Ni)	0.019	1,000	4.36	0.0044	-47.2
51. Netic 53-6	0.172	300	7.18	0.024	-32.4

For conductive coatings on glass or plastic substrates used for RF shields in which optical viewing is required where t is measured in nanometers (a tiny fraction of δ) the more stable, higher conductivity metals would be selected, such as gold.

2.6.2. Metallic and Other Conductive Coatings

Metals with lack homogeneity but which do not intentionally have holes, slits or other apertures are called pseudohomogeneous metals (PHM). Examples of PHMs include conductive paints and coatings and the arc or flame spray process of metalizing an insulator. A PHM may have thin areas because lack of adequate quality control of process does not lend itself to homogeneity. Consequently the theoretical SE of PHM may or may not correspond to measured results.

The principal techniques used for creating a conductive layer on top of an insulating material are the following:

1. Conductive paints
2. Plating (electrolytic)
3. Electrolyses plating
4. Flame spray
5. Arc spray
6. Ion (plasma torch) spray
7. Vacuum deposition

2.6.3. Small-Aperture Metals

Metals such as screens, metal mesh, conductive textiles which are called small-aperture metals (SAMs) do not follow the SE relations. In fact even if the bonding of the joints of screens were perfect the SE in terms of the resistance per square still would follow a different relationship at higher frequencies . At HF and above there is little evidence of the relationship of the base material conductivity and permeability of SAM to the SE in contrast to both homogenous and PHM. Except for some metalized textiles the SAM family may typically have from 1 to 1000 times as much air path as basic metal. These materials can constitute an enclosure by themselves (e.g. many of the first - generation shielded rooms were made with copper mesh) or the basis of some shielding integrity hardware (shielded glass, shielded ventilation panels, etc.) used to reduce the leakage of an existing hole in a conductive housing.

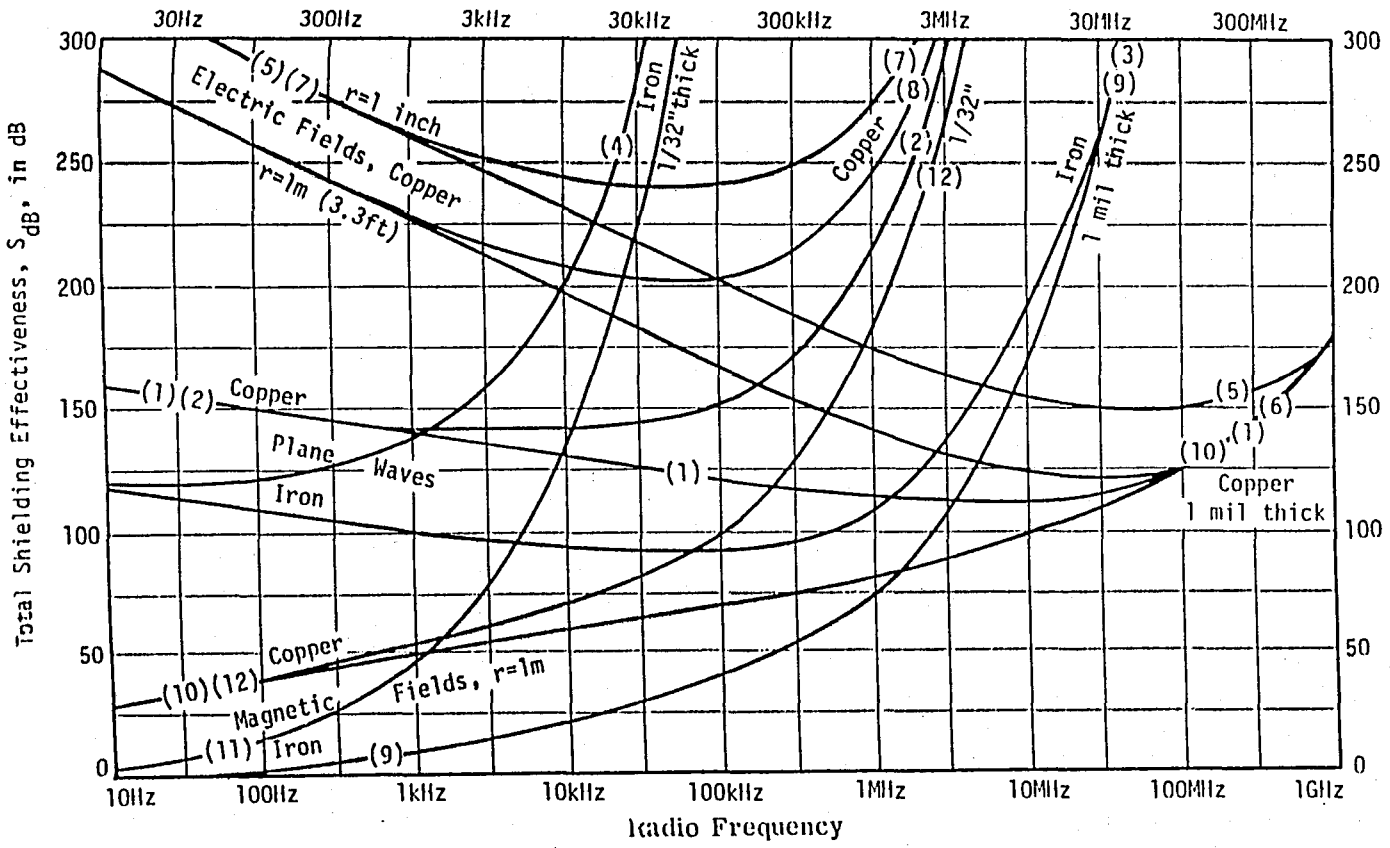

Figure 2.12. Total Shielding Effectiveness vs Frequency for Electric and Magnetic Fields and Plane Waves.

3. SHIELDING CHARACTERISTICS OF BUILDINGS

3.1. Cases in Need of Shielding

In a growing number of cases, some electromagnetic shielding is needed at the building level because of either the severity of the outside threat or the criticality of some system inside. Some examples are:

1. Buildings where EMI testing or other RF measurements are performed,

2. Hospitals using magnetic resonance imaging (MRI) scanners,

3. Buildings hosting some laboratories using electron beam microscopes, etc.,

4. Buildings housing ordinary electronic equipment, computers etc. and located near a powerful broadcast transmitter, radar or other noise source, since ordinary office computers can exhibit errors when exposed to field strengths exceeding 3 to 5 V/m particularly in the VHF band ,

5. Embassies, headquarters and govemment facilities handling confidential information which must be protected against eavesdropping.

This chapter shows that most buildings offer a fair (30 to 50 dB) attenuation to HF electric fields and very little attenuation beyond (see Fig. 3.1). If one wants to provide reliable shielding against strong ambient electromagnetic environments, it is necessary to use one form or another of screening on the exterior and, eventually, interior walls. Depending on the frequency range of concern and the amount of attenuation required, this may go as far as shielding and gasketing windows, doors, ventilation grilles, attics, etc. Very little reported data exists regarding tile mean attenuation of vehicles, aircraft and so on. However, this chapter presents some actual measured results as well as an analytical approach to determine SE.

3.2. Typical Building Attenuation

Two types of building attenuation are of interest:

1. SE versus frequency of exterior rooms located just inside the building facade

2. SE versus frequency of deep interior rooms which are protected by at least 30 m of inner walls, .corridors, etc.

Several measurement surveys were conducted. The surveys addressed ordinary unshielded buildings. The latter survey, incidentally, has been used as one of the data bases of CBEMA (Computer and Business Equipment Manufacturers' Association) study leading to the FCC-15J and CISPR-22 radiated EMI limits for computers.

Although a large variance appeared among the buildings surveyed, one can make several general observations:[10]

1. Predictably, brick, cinder and stone buildings with little or , no metal armature offer practically no low-frequency H-field attenuation. .

2. Steel-frame, multistory buildings exhibit a significant attenuation (50 dB average) in the AM range (a few hundred kilohertz).

3. Both E-field and H-field attenuations are at a null between approximately 50 and 200 MHz, where typical distance between girders is of the order of $\lambda/2$

4. There is a significant increase in attenuation in the center core of the building, where mean SE of more than 60 dB exists at 1 MHz.

5. Some of the measurements are inaccurate because power and telephone lines entering the building and reradiating can mask the actual building SE. For example, in a steel-frame building, you can pick up AM stations with a pocket radio, simply because the building attenuation is shunted by the power wiring reradiation.

6. Most of the measurements were performed using remote external sources, i.e. the myriad of broadcast fields as reference. No information seems to be available concerning the reverse, i.e. the SE of a building for sources located inside. It can be assumed that this attenuation will be poorer since sources will create near H-field situations (lesser reflection SE) and also will be closer to the building apertures.

Fig. 3.1. is a plot of the fitted mean values of building SE. Compared to the large data base available, here is a standard deviation of +10 to 15 dB (depending on frequency) around these mean values.

3.3. Exterior Building Materials

The exterior of most buildings is either cinder block, concrete or brick. Less frequently, exteriors are of wood, glass or stone.Studies conducted by the National Bureau of Standards (NBS) showed that the median SE for a single-layer brick wall is only 2.5 dB between 500 and 1,000 MHz. Above I GHz, absorption loss becomes significant because even a poorly conductive clay or concrete will have a skin depth of about 10 cm at 1GHz. An interesting material is coke, which offers a typical dc resistivity of 0.1 ohm-centimeters (Ωcm) at dc. Therefore, a thick layer of coke chunks can achieve some reflection and absorption above HF. Typical SE of a 30 cm layer of coke chunks about 30 cm in diameter is 60 dB at 100 kHz (plane waves) to 90 dB at 1 GHz. These numbers are for untreated coke. Treated coke, where the sulphur content has been extracted, still shows 50 dB at 100 kHz to 70 dB at 1 GHz per 30 cm thickness.

One approach to using coke as a building shielding material is to pour coke dust or granules between two layers of back, concrete slabs, or behind a wooden siding. However, typical architectural practices do not allow a 30 cm waste in the thickness of each wall, and only 5 or 10 cm can be reasonably accommodated. This provides only 10 to 20 dB of SE-hardly an impressive figure.

Another approach would be to manufacture bricks, cinder blocks, etc., with a specified percentage of coke dust, such that structural strength is not significantly affected. Here again, this would probably just give about 10 to 20 dB per 30 cm thickness.

One obvious solution to improve the RF attenuation of the facade is to use a conductive top coat such as aluminum foil, conductive textile or conductive paint. For example, a minimum SE of about 50 dB can be achieved by using aluminum foil. To do this, the wall must be dressed to provide a flat surface for the application of the foil. This can be done by using furring strips overlaid with 1 cm plywood, particle board or gypsum boards. Aluminium foil, 60 μm thick and in rolls about 1.20 m wide, can be installed like wallpaper and overlapped about 10 cm on the edges. It is then affixed with staples on 10 cm centres. A strip of ordinary nonconductive adhesive tape can be rolled over the edges for mechanical protection. The underlayer must be thick enough to prevent the staples from touching any metal in the building which may be connected to an earthing conductor.

A second foil is laid over the first layer and stapled. This layer is offset by half a layer width so that the edges of the second layer fall in the middle of the first one. All the inside comers of the rooms must be covered first so that there are no seams at the comers. A single 1 cm crack can compromise the whole building SE at as much as 50 dB at 500 MHz.

The next problem is matching the foil to the door stills and the room floor and ceiling. Ideally, these should be made of sheet metal, too, or installed with an underlayer of wire screen below the floor and above the ceiling boards.

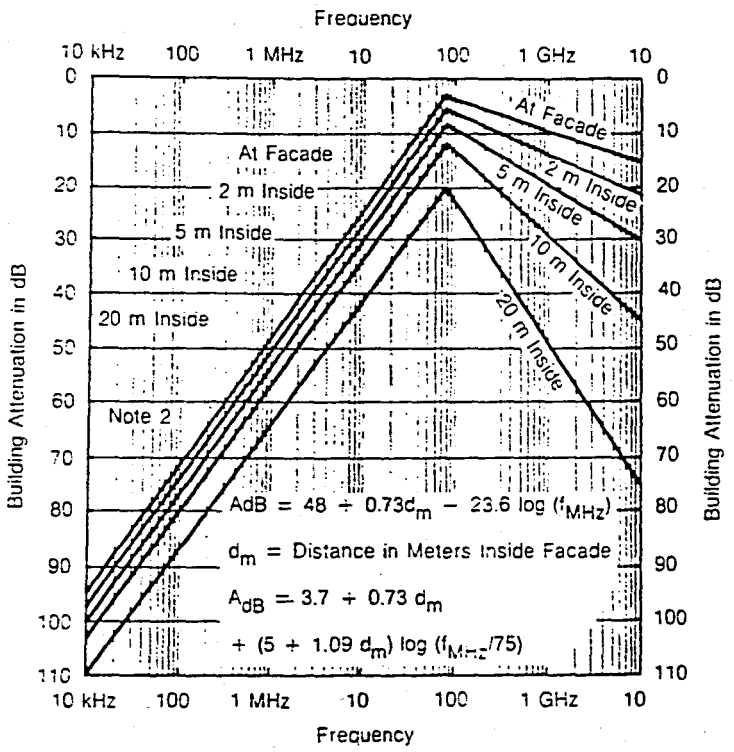

Notes: 1. Buildings surveyed are business-type, with metal girders.
2. Suggested extrapolation for E-Field Attenuation—H-Field attenuation decreases significantly below 1 MHz, to approach 0 dB around 10 kHz.

Figure 3.1. Building Attenuation to Outside Radiations vs. Frequency and Distance Inside Facade [8]

A better installation can be made using copper foil backed by a material similar to roofing paper and glued to the underlayer boards. Conductive copper tape can be used to seal the seams. Copper tape strips can extend down at regular intervals to connect to the floor. Finally, a horizontal strip is criss crossed with the vertical strips. The same technique can be used to bond the conductive foil to the door and window frames.

Another material developed by Fortifiber Corp, of Attleboro, MA. is a copper armored sisalkraft constructed of a 3 oz (0.1 mm thick) copper sheet laminated to a heavy-duty fiberglass reinforced kraft paper. The fiber mesh gives the material the physical strength to withstand construction job abuse. The kraft backing facilitates gluing to the walls. The seams are bonded with copper tape which is soldered to the 3 oz copper sheets.

Looking at the performance of wire meshes and textiles, we see that a thin mesh (e.g., 22 wires/inch, approximately corresponding to 1 mm openings) provides more than 60 dB up to 100 MHz. These screens or fabrics can be impregnated in plaster or concrete during construction or laid over the walls for post-construction shielding. The installation procedure is similar to that for wallpaper and follows the guidelines described previously for aluminium foil. Ceilings and floors can be covered with mesh, which is overlapped slightly (10 cm) at the walls and comers. Then the ceiling and floor can be covered as usual. Installers must take proper precautions so that lighting fixtures do not pierce or deteriorate the ceiling mesh.

While expensive when compared to normal construction, such "Faradization" of a building section is considerably cheaper than installing even the least sophisticated shielded room. While conductive paints would be an interesting alternative, and much easier to apply, they are not widely used. One possible reason is the relative fragility of such a thin coating over an interior wall: it can be easily scratched, peeled and abused in many ways. Most people would not suspect the consequences of a scar a few centimetres in width.

3.4. Treatment of Doors, Windows and Other Openings

Above a few megahertz, the SE performance of a building will be dominated by the penetrations. All openings such as windows and doors, though surrounded with conductive materials or a steel structure, will be RF transparent when their larger dimension reaches $\lambda/2$, i.e. at approximately 75 to 100 MHz. Hollow-core steel or aluminium doors can be used. Finger-stock gasketing should be used to seal the door periphery if better than 60 dB SE is required up to 1 GHz. Otherwise, cheaper conductive gaskets can be used. Windows should be equipped with screen-type glass panels with a conductive strip around the entire edge to make contact with the window frame When SE has to be improvised on the spot, screen mesh or metalized textile can be laid over the window and folded over at the edges to make contact with the frame.

Other penetrations, can be equipped with screen vents or stretched metal grids. If better than 60 dB is required, or if the purpose of the shielding is to contain confidential information within government offices, embassies, etc., screen vents are insufficient.

Finally, other penetrations include water, sewage and other utility lines. Where nonconductive pipes are used, another technique is applied by welding or fitting a heavy galvanised steel or copper pipe through a flange mounted over the surface of a conductive - panel. Because this method cannot work when a conductor is driven inside, a power line filter must be used on incoming ac wiring such that all lines including the neutral are filtered. The same applies to telephone or other data lines (local area networks etc.).

Single-point grounding of each of these improvised shielded rooms is maintained by isolating grounded plumbing and pipes. This is accomplished by using dielectric sections of approximately 10 cm long pipe which is inserted into the plumbing and other metal pipes. Then the wall shielding is connected to the room power panel ground bus (safety earth) via a single green-yellow (solid green in the United States) well-identified insulated wire. When more attenuation is required, like 80 or 100 dB, it is almost mandatory to contract out either the construction of a custom made shielded room, or to install a prefabricated shielded room inside the building.

3.5. Shielding Effectiveness of Various Buildings

Shielded rooms are designed to achieve specific levels of attenuation and are used principally for EMI measurements and to contain classified electronic information or restricted transmissions. In this section we examine the shielding effectiveness of commercial buildings and residential houses. The reduction in the signal strength of a radio transmission as it propagates inside a building is undesirable when reception is required. Most of us have noticed the reduction in signal strength as a portable radio is moved from a position close to a window to further inside the building. However building attenuation is a desired attribute when the source of the field is either high level broadcast transmissions, lightning or radar which have the potential for interference.

In an EMC/EMI investigation which includes a building in the radiated propagation path, data on the average attenuation for different types of buildings is required. When susceptible equipment is contained in the building then the magnitude of the field incident on the building may be predicted from the distance and source characteristics. When the building is used to shield a receptor from a source then the diffraction of the wave around the building must be accounted for in addition to attenuation through the building.

As noted in enclosure shielding the E field and H field component may not be equally attenuated by a material and the wave impedance may change after transmission through a medium.

Both the E and H fields of ambient broadcast signals were measured inside and outside seven different types of buildings in [1]. The seven types of building were

1) Single family detached residence of the split level ranch type. Materials: wood framed with wood and brick siding, aluminium foil covered insulation in the ceiling.

2) Single family detached residence of the wood framed raised ranch type. Materials: Concrete block walls on the lower levels and aluminum siding covering the upper levels. Brick veneer from on the main level.

3) Single story concrete block. Materials:Concrete blocks with a large store front window. Structure framed with steel columns and a steel bar joist supported roof, Interior divided into cubicles with demountable steel and glass. An extensive array of ducts, pipes and cables occupied the space above a suspended ceiling.

4) Single story concrete block. Materials: Concrete block steel framed building constructed on a reinforced concrete slab. Interior description similar to 3.

5) Four story office. Materials: Steel framed with preformed concrete extenor wall panels, One side covered with metal exterior wall panels. The floors are corrugated steel covered with poured concrete. The interior description similar to 3.

6) Four story office. Materials: Steel frame with brick exterior walls. Corrugated steel floors covered with poured concrete. Interior description similar to 3.

7) Twenty story office. Materials: Steel frame with marble exterior wall panels. Interior steel columns spaced approximately 7 m apart. Corrugated steel floors covered with poured concrete. The interior is uncluttered with few interior walls and partitions.

The level of attenuation depends on the interior location at which the measurement was made. Thus measurements were made at a number of different locations in each building. Table 3.2 provides a summary of the fitted mean, minimum and maximum measured attenuation of the seven buildings.

The attenuation of UHF radio signals by buildings has been measured in [10]. Table 3.3 is a summary of the effects of frequency and building type on the attenuation. The average attenuation from measured data is 6.3 dB. The table shows correction factors which must be added to or subtracted from 6.3 dB to account for frequency, room location and building materials used in the construction.

When equipment housed in a building is found to be susceptible to a source of high power radiated emissions, such as a transmitter, and it can be proven that the EMI problem is marginal, then a few dB of additional attenuation may be all that is required to eliminate EMI. The first step in such an investigation is to prove that the coupling path is truly radiated to the equipment inside the building and not radiated to nor conducted on external power or signal lines. The next step is to ensure that a modicum of additional shielding is all that is required.

One method of enhancing the building attenuation is to paint it with conductive paint. For example a powdered nickel acrylic base conductive paint was used on concrete or concrete block walls. The measured attenuation after painting increased by 20 dB over the 100 MHz to 350 MHz frequency range and 16 dB for the pulsed field from lightning. Additional shielding at windows may be achieved by the use of wire mesh in a frame which is electrically connected to the conductive paint. A transparent plastic film coated with

copper or gold may also provide sufficient shielding at windows but is a more costly solution and care must be taken to ensure that the conductive side of the film contacts the paint either directly or via a metal window frame.

Table 3.1. Building Attenuations [1]

Building	Frequency	H field mean [dB]	H field limits [dB]	E field mean [dB]	E field limits [dB]
1	20 kHz	0	-	32	-
	1 MHz	0	-	30	-
	500 MHz	0	-5 to 3	0	-5 to 8
2	20 kHz	3	-	22	12 to 33
	1 MHz	0	-5 to 2	9	-8 to 4
	500 MHz	10	2 to 20	12	7 to 20
3	20 kHz	-1	-	*	-
	1 MHz	3	-	18	-
	500 MHz	8	-3 to 19	8	-3 to 15
4	20 kHz	-3	-	-	-
	1 MHz	12	5 to 25	28	12 to 28
	500 MHz	8	-	10	-
5	20 kHz	2*	-	-	-
	1 MHz	3*	-	22*	-
	500 MHz	6*	-	3*	-
6	20 kHz	3*	-	32*	-
	1 MHz	8*	-	28*	-
	500 MHz	10*	-	10*	-
7	20 kHz	20*	-	40*	-
	1 MHz	20*	-	35*	-
	500 MHz	10*	-	10*	0 to 25*

Not: The values marked with * were measured 1 m from the outer wall of the buildings. Measurements made 15 m from the outer wall showed attenuation of up tc 35 dB for magnetic fields and up to 50 dB for electric fields. Mobile homes provide an average of 28 dB of attenuation over the 20 kHz to 500 MHz frequency range.

Table 3.2. Attenuation Correction Factors.

		Correction factor* [dB]
Frequency	2569 MHz	1.160
	1550 MHz	0.390
	860 MHz (V)	-0.169
	860 MHz @I)	0.140
Construction	Wood siding	-0.58
	Brick veneer	0.58
Insulation	Blown in ceiling	-0.8
	ceiling and walls	0.8
Room position	Exposed walls	0.3
	No exposed walls	0.3

Note: * Average attenuation from which the following correction factors are added/subtracted is 6.3 dB.

When a higher level of shielding than achievable with conductive paint is required then the use of sheets of metal foil soldered or taped together on the inside walls and ceiling is an alternative. Earth is a good absorber of electromagnetic radiation, therefore installing equipment below ground level and/or building up a 2 m thick wall of earth around the room housing the equipment is another potential solution.

4. MULTILAYER STRUCTURES

4.1. Theory

The basic problem considered in this part of the thesis is the electromagnetic interaction (reflection and transmission) of a plane incident electromagnetic wave with multilayer.

Assuming that at any point (x,y,z) of a layer, reflection and transmission wave of the incident plane wave can be used to derive a set of four recursion formulas each of which is valid for an arbitrary layer number of multilayer and for arbitrary angle of incidence.

Since either the electric field intensity vector (Case I), or the magnetic field intensity vector (Case II) is parallel to the plane interfaces four scaler quantities can be introduced by means of which the four recursion formulas can then be developed. With reference to Fig. 4.1 these are

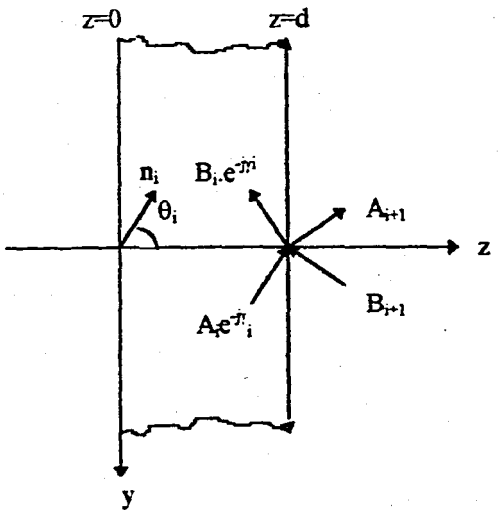

Figure 4.1. The ith layer of a multilayer structure.

A_i Tangential E at left interface of ith layer, travelling left to right

B_i Tangential E at left interface of ith layer, travelling right to left

F_i Tangential H at left interface of ith layer, travelling left to right

G_i Tangential H at left interface of ith layer, travelling right to left [11]

At each interface, four field components are generaly present. As shown in Fig. 4.1. at the right interface of the ith layer two waves are travelling left to right and two waves are travelling right to left.

The exponential decribing $e^{\pm j\gamma i}$ these waves take into account both the attenuation and phase shift of the waves as they go through each layer. More presicely the wave travelling left to right is represented by an expression of the form $A_i e^{-j\gamma_i \cdot n_i \cdot r}$ where n_i is the two dimensional vector $\mathbf{n_i} = -\sin\theta_i \mathbf{a_y} + \cos\theta_i \mathbf{a_z}$ and r denotes the usual position vector $\mathbf{r} = x\mathbf{a_x} + y\mathbf{a_y} + z\mathbf{a_z}$.[12]

Additionaly, γ_i is the complex propagation constant for ith layer.Without loss of generality all observation can be made in the plane y=0. Then $\mathbf{n_i}.\mathbf{r} = z.\cos\theta_i$ and the wave travelling left to right becomes $A_i e^{-\gamma_i z \cos\theta_i}$ .The development of an expression for the wave traveling right to left follows a similar course, with the corresponding result $B_i e^{\gamma_i z \cos\theta_i}$. The angle θ_i is determined from a consideration of the boundary conditions at the respective interfaces. For case I, continuity of the electric field intensity at z=d requires that

$$A_i e^{-k_i} + B_i e^{k_i} = A_{i+1} + B_{i+1} \tag{4.1}$$

where

$$k_i = \gamma_i d_i \cos\theta_i \tag{4.2}$$

For the magnetic field continuity implies a more complex result. Let us consider Fig.4.2(a). We see that just to left of the interface the tangential H field is

$$H = (H_i \cos\theta_1) - (H_r \cos\theta_1) \tag{4.3}$$

or in terms of the intrinsic impedance of the medium,

$$H = \frac{1}{n_1}\left[(E_i \cos\theta_1) - (E_r \cos\theta_1)\right] \tag{4.4}$$

This expression automatically assumes that the angle of incidence is equal to the angle of refraction or, that Snell's law are valid. If this assumption is carried over to the case when

there is a wave travelling right to left in medium 2 of Fig. 4.2 (a) then in the case we are considering we can write

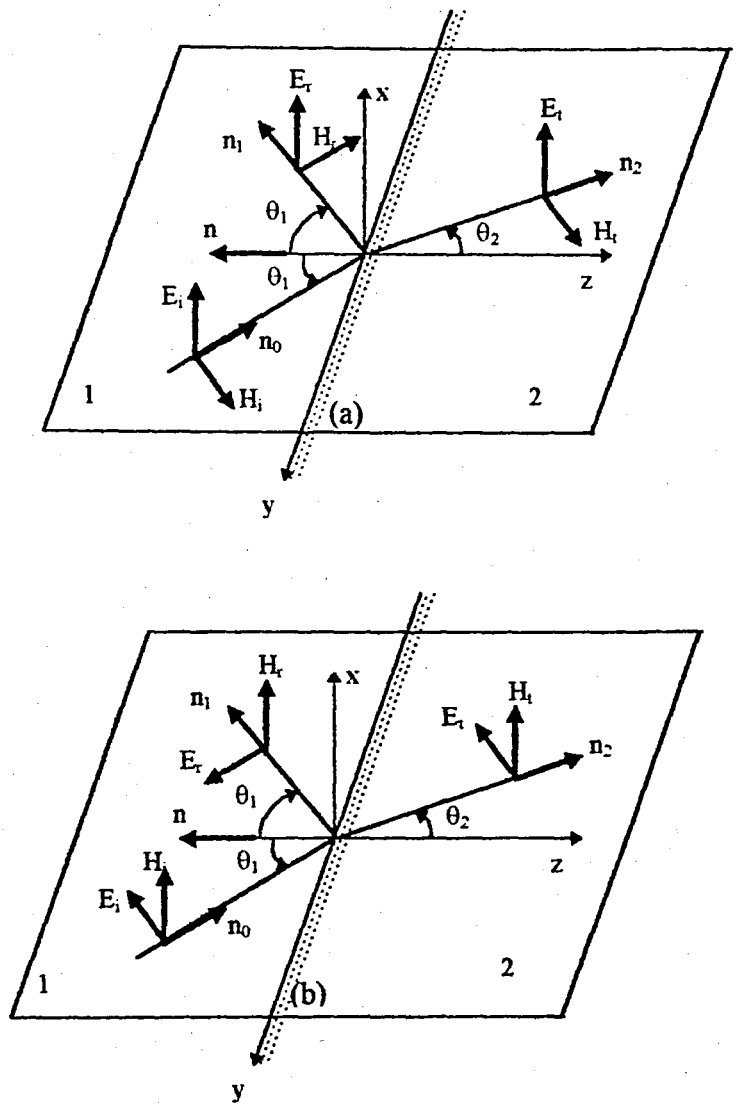

Figure 4.2. Oblique incidence (a) E_i parallel to interface; (b) H_i parallel to interface

$$\frac{\cos\theta_i}{n_i}\left(A_i e^{-k_i} - B_i e^{k_i}\right) = \frac{\cos\theta_{i+1}}{n_{i+1}}\left(A_{i+1} - B_{i+1}\right) \tag{4.5}$$

where

$$n_i = \sqrt{\frac{jw\mu_0}{\sigma_i + jw\varepsilon_i}} \tag{4.6}$$

The assumption that Snell's laws hold in this case assures us that the tangential fields are in phase with each other everywhere on the boundary. Furthermore, it allows us to compute the angle θ_i from

$$\gamma_0 \sin\theta_0 = \gamma_1 \sin\theta_1 = \cdots = \gamma_i \sin\theta_i = \cdots = \gamma_N \sin\theta_N = \gamma_{N+1} \sin\theta_{N+1} \tag{4.7}$$

The remaining part of the problem involves pure algebraic manipulations. We can obtain [4]

$$\frac{n_i}{n_{i+1}} = \sqrt{\frac{\sigma_{i+1} + jw\varepsilon_{i+1}}{\sigma_i + jw\varepsilon_i}} = \sqrt{\frac{\varepsilon_{i+1}(1 - j\tan\delta_{i+1})}{\varepsilon_i(1 - j\tan\delta_i)}} \tag{4.8}$$

and

$$Y_{i+1} = \frac{\cos\theta_{i+1}}{\cos\theta_i} \sqrt{\frac{\varepsilon_{i+1}(1 - j\tan\delta_{i+1})}{\varepsilon_i(1 - j\tan\delta_i)}} \tag{4.9}$$

gives

$$A_i e^{-k_i} - B_i e^{k_i} = Y_{i+1}(A_{i+1} - B_{i+1}) \tag{4.10}$$

which when added and subtracted to the previously derived Eq. (4.1) gives the desired results:

$$\begin{bmatrix} A_i \\ B_i \end{bmatrix} = \frac{1}{2} \begin{bmatrix} e^{k_i} A_{i+1} & e^{k_i} B_{i-1} \\ e^{-k_i} B_{i+1} & e^{-k_i} A_{i+1} \end{bmatrix} \begin{bmatrix} 1 + Y_{i-1} \\ 1 - Y_{i-1} \end{bmatrix} \tag{4.11}$$

where

$$k_i = d_i \gamma_i \cos\theta_i \tag{4.12}$$

$$\gamma_i^2 = -w^2 \mu_i \varepsilon_i + jw\mu_i \sigma_i \tag{4.13}$$

then

$$k_i = d_i \cos\theta_i \sqrt{-w^2 \mu_0 \varepsilon_i + jw\mu_0 \sigma_i} = \frac{d_i}{\lambda_0} \cos\theta_i \, 2\pi \sqrt{\varepsilon_{ri}(-1 + j\tan\delta_i)} \tag{4.14}$$

and θ_{i+1} is the complex angle of refraction in ith layer and obtain by [4]

$$\theta_{i+1} = \sin^{-1}\left[\frac{\gamma_i}{\gamma_{i+1}}\sin\theta_i\right] \qquad i=,0,1,2,..,N \qquad (4.15)$$

Now in the region of the right of the multilayered slab, there is only a wave travelling left to right whose amplitude can arbitrarily be set equal to unity. Therefore if we set $A_{N+1}=1$ and $B_{N+1}=0$, we can determine expressions for A_i and B_i, in sequence, by setting i=N,N-1,... ,2.1.0 in the recursion formulas above. Obviously, A_0 is the incident wave on the left of the slab, and B_0 is the reflected wave. As a result,

$$R_{\perp} = \frac{B_0}{A_0} \quad , \quad T_{\perp} = \frac{1}{A_0} \qquad (4.16)$$

The analysis follows similare course for Case II with only slight changes in natation and requires the use of Fig. 4.2(b) to derive expression for boundary conditions. $F_{N+1}=1$ and $G_{N+1}=0$,

$$W_{i+1} = \frac{\cos\theta_{i+1}}{\cos\theta_i}\sqrt{\frac{\varepsilon_i(1-j\tan\delta_i)}{\varepsilon_{i+1}(1-j\tan\delta_{i+1})}} \qquad (4.17)$$

$$\begin{bmatrix} F_i \\ G_i \end{bmatrix} = \frac{1}{2}\begin{bmatrix} e^{k_i}F_{i+1} & e^{k_i}G_{i+1} \\ e^{-k_i}G_{i+1} & e^{-k_i}G_{i+1} \end{bmatrix}\begin{bmatrix} 1+W_{i+1} \\ 1-W_{i+1} \end{bmatrix} \qquad (4.18)$$

$$R_{II} = \frac{G_0}{F_0} \quad , \quad T_{II} = \frac{1}{F_0} \qquad (4.19)$$

Finally

$$R_{\perp}^2 = \left[\mathrm{Re}(B_0/A_0)\right]^2 + \left[\mathrm{Im}(B_0/A_0)\right]^2 \qquad (4.20)$$

$$T_{\perp}^2 = \left[\mathrm{Re}(1/A_0)\right]^2 + \left[\mathrm{Im}(1/A_0)\right]^2 \qquad (4.21)$$

$$R_{II}^2 = \left[\mathrm{Re}(G_0/F_0)\right]^2 + \left[\mathrm{Im}(G_0/F_0)\right]^2 \qquad (4.22)$$

$$T_{II}^2 = \left[\mathrm{Re}(1/F_0)\right]^2 + \left[\mathrm{Im}(1/F_0)\right]^2 \qquad (4.23)$$

In either case , we defined reflection coefficient R as the ratio of reflected (E_r) to incident (E_0) field intensities in the free space to the left of the first plane boundary; also we

defined transmission coefficient as the ratio of the transmitted (E_t) field intensity in the free space to the right of the last plane boundary to the incident field intensity (E_o). Thus

$$R_{\perp}=\left(\frac{E_r}{E_o}\right)_{\perp} \quad , \quad T_{\perp}=\left(\frac{E_t}{E_o}\right)_{\perp} \tag{4.24}$$

$$R_{||}=\left(\frac{E_r}{E_o}\right)_{||} \quad , \quad T_{||}=\left(\frac{E_t}{E_o}\right)_{||} \tag{4.25}$$

4.2. Verification of the Multilayer Model: A Comparison of Computer Code Results With Previous Studies

The result of section 4.1 were used to calculate shielding effectiveness of the different multilayer structure[3], [4], [11]. Using the multilayer program running on the MATLAB works correctly, [3] and [4] studies had been examined again before comparing the outputs of the program with the experimental results. The same results were obtained with these studies as seen by graphic outputs in this section.

4.2.1. Testing of the Computer Program

4.2.1.1. Testing for Effects of the Incident Angle

For the verification; the computer code was firstly applied to a problem given in the "Basic Electromagnetic Theory" [4] The effect of the incident angle and the material properties of each layer were analized and we obtained the same values as the result of [4]. Therefore, it can be safe to say that this program calculates the correct values for the multilayer structures.

Table 4.1 gives characteristic values of each layer for five layers at the 300 MHz. with incident angle 0^0 to 90^0 .

Table 4.1. Characteristic Values of Each layer

EPSR (ε_r)	CLTN ($\delta=\sigma/\varepsilon_r\omega$)	DL (di/λ_0)	PRR (μ_r)
1.00	0.000000	0.0000	1.00
4.30	0.015000	0.0406	1.00
1.15	0.005000	0.1355	1.00
4.30	0.015000	0.0406	1.00
3.15	0.035000	0.0180	1.00
7.30	0.270000	0.0027	1.00
1.00	0.000000	0.0000	1.00

For these input values results given below as Table 4.2 are the same results with [4].

Table 4.2. Transmission and Reflection Coefficient for each Incident Angle

ANG	TPE2	RPE2	TPA2	RPA2
0.0000	0.91613	0.00952	0.91613	0.00952
10.0000	0.91576	0.00908	0.91824	0.00839
20.0000	0.91325	0.00923	0.92185	0.00776
30.0000	0.90344	0.01533	0.92281	0.01162
40.0000	0.87464	0.03950	0.92318	0.01672
50.0000	0.80475	0.10517	0.93254	0.01225
60.0000	0.66088	0.24860	0.94861	0.00023
70.0000	0.42062	0.49923	0.89387	0.06116
80.0000	0.13913	0.81063	0.50452	0.46572
90.0000	0.00000	1.00000	0.00000	1.00000

where TPE2= T^2 for E Field

RPE2= Γ^2 for E field

TPA2= T^2 for H Field

RPA2= Γ^2 for H Field

4.2.1.2. NEMP - Interaction with Plane Multilayer Structures.

In the [3] electromagnetic pulses, their characteristics and effects on layered media were investigated using a multilayer structure as given in Fig.(4.3)

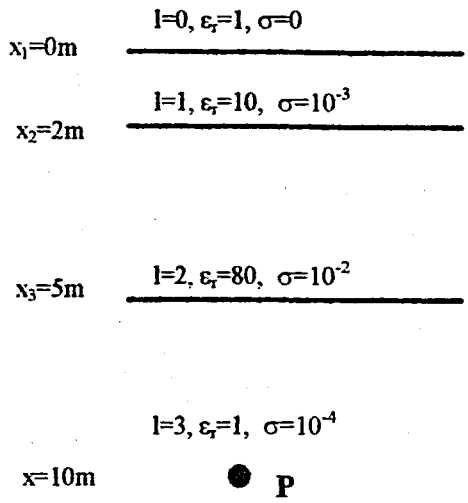

Figure 4.3. Multilayer Structure used in Ref. [3]

The electromagnetic fields at an observation point P (x=10m) in frequency domain (1 kHz to 100MHz) were computed considering normal incidence and incident angle of 30, 60 and 85 degrees for both electric and magnetic fields and also by setting ε_r=10 for the rock. After that the shielding effectiveness for the same point P is calculated.

Table 4.3. Layer Charecteristics of Fig. 4.3.

CHAR / MEDIA	ε_r	ε_i	μ_r	μ_i	σ	d
AIR	1	0	1	0	0	0
DRY SOIL	10	0	1	0	10^{-3}	2m
GROUND WATER	80	0	1	0	10^{-2}	5m
ROCK	1	0	1	0	10^{-4}	10m

Figure 4.4-4.8. show the simulation results of the Figure 4.3.

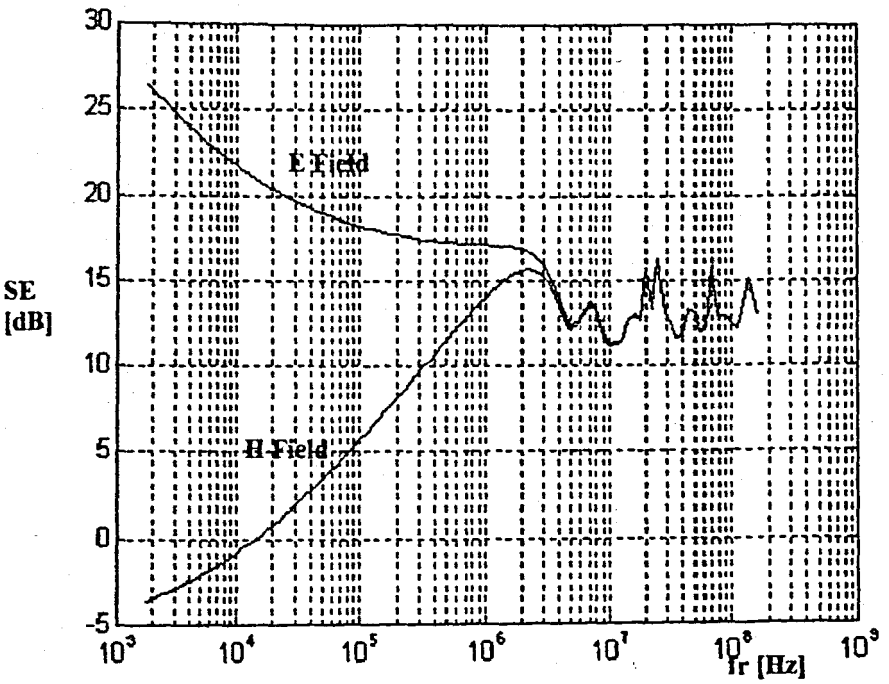

Figure 4.4. SE versus frequency for incident angle=0, ε_r=1, $\sigma=10^{-4}$

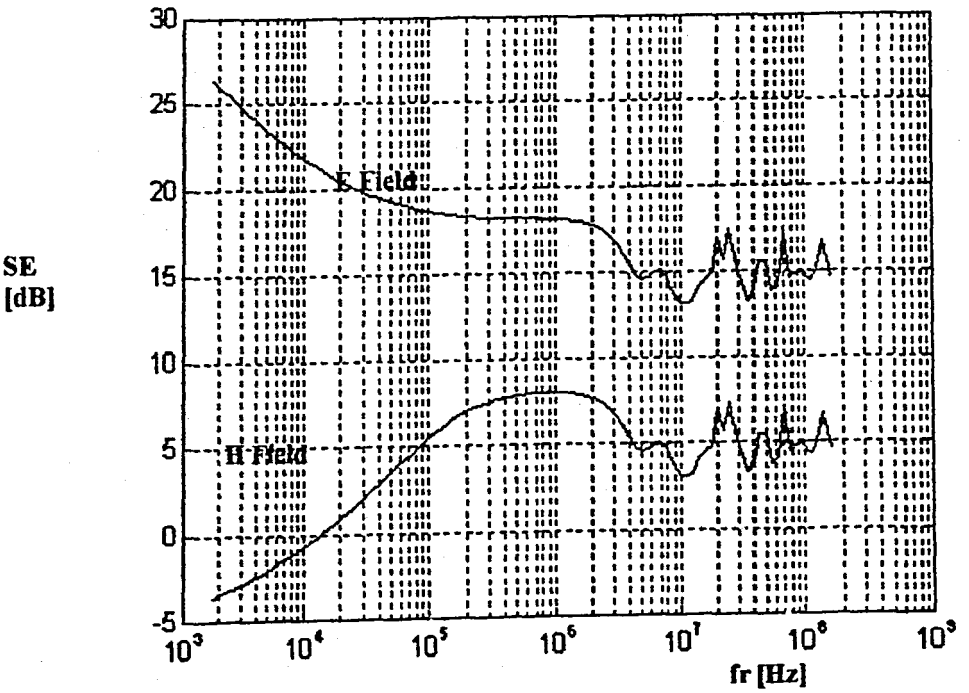

Figure 4.5. SE versus frequency for incident angle=0, ε_r=10, $\sigma=10^{-4}$

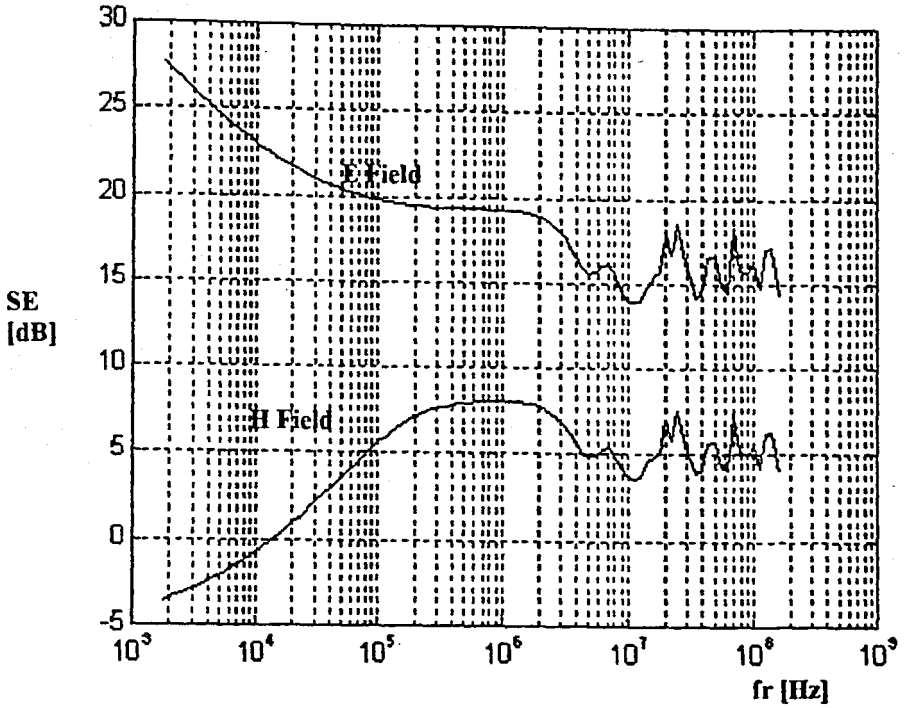

Figure 4.6. SE versus frequency for incident angle=30, ε_r=10, σ=10^{-4}

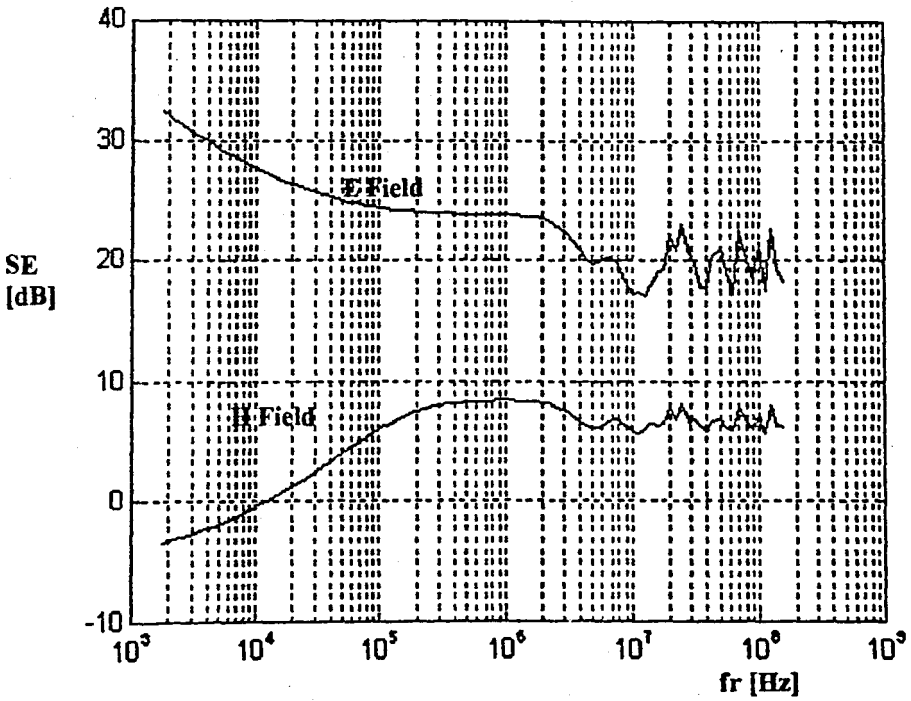

Figure 4.7. SE versus frequency for incident angle=60, ε_r=10, σ=10^{-4}

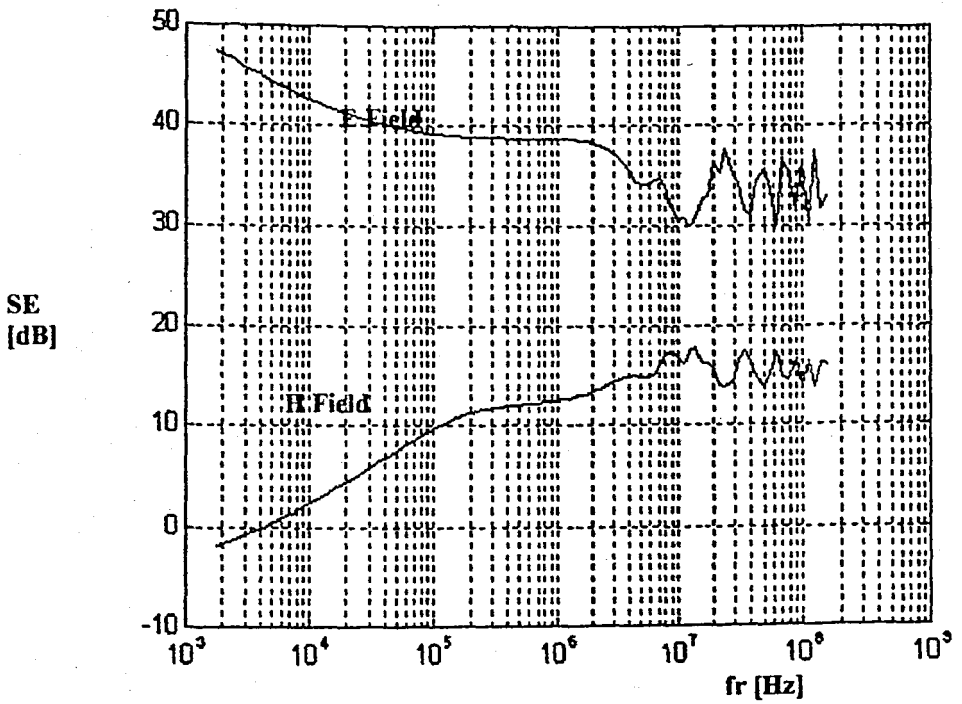

Figure 4.8. SE versus frequency for incident angle=85, ε_r=10, σ=10^{-4}

4.3. Multilayer Model for a Single Floor

The model as presented above gives us the transmission and reflection coefficients of the layers. According to formula given in Chapter 2 shielding effectiveness is calculated from Eq. (2.13) . This equation is also a transmission coefficient of the electromagnetic field power. We can easily say that transmission coefficient of the multilayer can be used for calculating the shielding effectiveness of the layers.

Firstly, rooms housed through a corridor in the same floor can be modelled as a multilayer structure. This model can be easily adopted to the program. Parameters which are needed for calculating SE (μ_r, σ_r, ε_r and the distance for the measurement point) are known for this building. So therotical results are obtained using this program for seven rooms at 200-1000 MHz. In order to achieve measurement and store data, an automated measurement system is used. When we apply this model in a building, we must deal with some scattering and diffraction terms as well. On the same floor calculation, diffraction term

is less significant than the reflection and transmission termand received electric field strength is given .[5]

$$|E_i|^2 = \frac{Z_0 P_e}{4\pi L^2} \prod_n \Gamma_n^2 \prod_m T_m^2 \qquad (4.26)$$

where P_e is the effective radiated power and Z_0 is the freespace wave impedance Γ_n , T_m are the magnitudes of reflection and transmission coefficients of the wall. For the 200 MHz-1000 MHz frequency range, 0.5 W output power relative permeability of wall μ_r=1 , relative conductivity of wall σ_r=0.015 and relative permitivity of wall εr=12 reflection coefficient (Γ_n), transmission coefficient (T_m) are calculated from multilayer model. Results are given in Chapter 5 together with the same graph of the measurements results.

Buildings represent a complex environment of very large dimensions compared to wavelength. Besides the basic building structure (walls, floors and ceiling), furnishings and people serves as a scatterers of radio wave. Because the many propagation paths from transmitting to receiving antenna result from of scattering events, the paths exhibit many different starting directions at the transmitting antenna and many different directions of arrival at the receiving antenna. The resulting multipath structure causes the received signal to exhibit strong variations as either the transmitting or receiving antenna is moved over a distance on the order of $\lambda/2$. For propagation inside buildings traditional practise has been to avarage the signal by moving the transmitter or the receiver over a spatial area having linear dimension of 10 to 20 wavelengths (often in a circular path) to remove the rapid variation . The result has been referred to as the sector average.

In this case since we consider the only the transmitting and receiving antenna on the same floor, the large scale geometry includes two features that can be treated independently. The first is the vertical clear space between floor and ceiling or between furnishings and ceiling through which the fields can propagate. The second consists of the walls at which reflection and transmission of the signal take place.

The vertical propagation space in which a signal can propagate depends on environment of the building. Typical office buildings will have rooms filled with desk, chair file cabinets, low partitions etc. That define the lower boundary of the clear space through which the signal can propagate. The upper boundary of this clear space is defined by

support beams, pipes ventilation ducts lighting fixtures. These features are often hidden by an acoustic drop ceiling whose tiles have little effect on UHF signals. For a signal propagating through the rooms of an office building the vertical propagation space will be between the furniture and the ceiling features typically 1.5-2.5m.

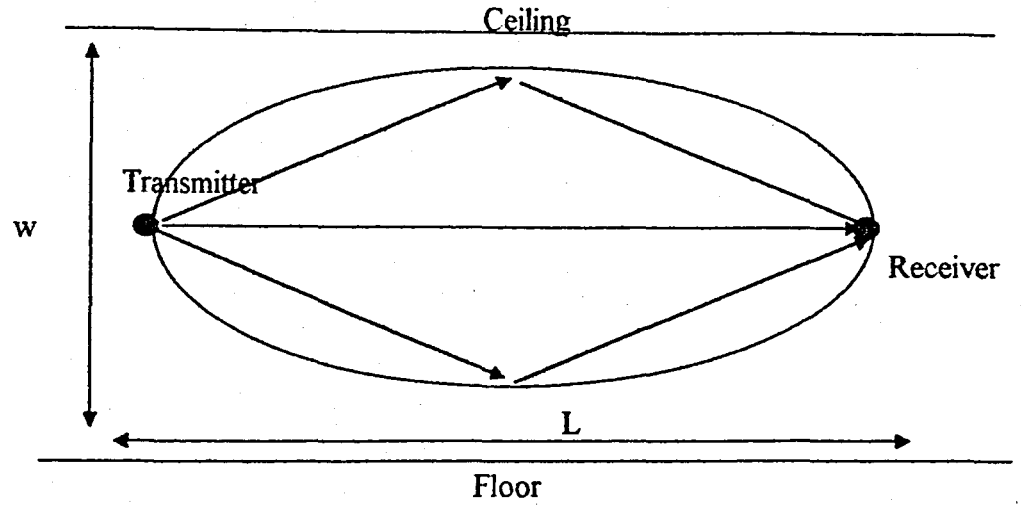

Figure 4.9 Clear Space (w)

For propagation to distant points it is only the forward scattering through small angles that is significant. Fields resulting from scattering that occurs at large angles will influence the local interference pattern. However to contribute at distant locations the fields would have to be rescattered through large angles there by further reducing their amplitudes. Forward scattering is not sensitive to the shape of the object or bondary conditions. (Fig. 4.9.) The change in excess path loss can be understood with reference to the with of the first Fresnel zone for the source and receiver antenna at the mid point of the clear space. The full width w_f of the Fresnel zone is approximately given by $w_f = \sqrt{\lambda . L}$. For example for seperations less than 12m at a frequency of 900MHz $w_f < 2m$ so that the Fresnel zone lies with in the clear space and the presence of the scattering features influence the propagation between transmitter and receiver leading to excess path loss. For antenna located closer to the floor or ceiling, the Fresnel zone touch the upper or lower boundaries at antenna seperation distances L shorter than when the antennas are directly in the middle of the clear space and may lead to differences in the excess path loss.

In our program since frequency varies from 200 MHz-1000 MHz and L changes from 3m to 30 m clear space distance w is not constant. In this aspect measurement conditions are not always same.

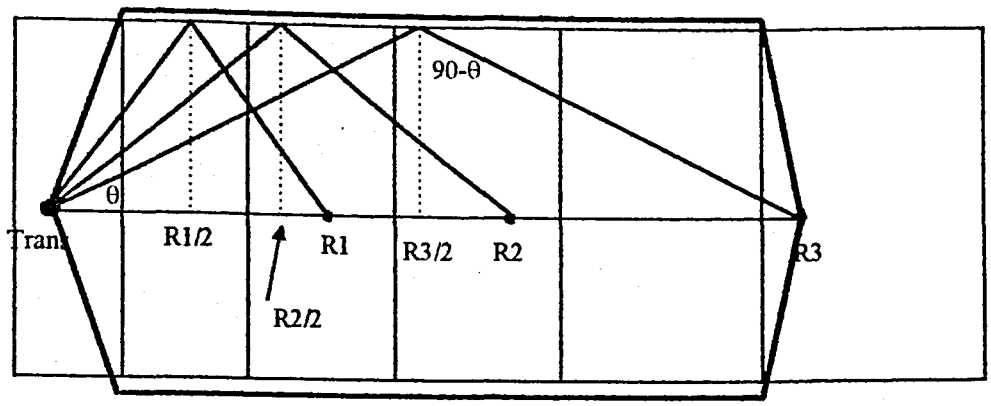

Figure 4.10 Reflection from Wall

Figure 4.9. shows the effects of the reflected wave from floor and ceiling and Figure 4.10 shows the effects of the side walls. Both vertical and horizantal space the transmitted waves pass through the inside walls. Because of the Snell Laws transmitted waves pass the other side of the each wall as the same angle with incident wave. (Figure 4.11) Therefore we can easily apply these reflection terms in the multilayer program as a multiplier.

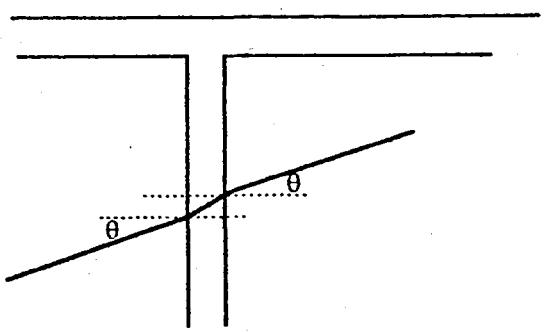

Figure 4.11 Transmiting wave from only one wall

4.4. Multilayer Model for Separated Floors

In order to examine the propagation characteristics between floors of a building the possible paths of propagation must be determined.[6] Two paths over which propagation can take place are (a) paths that involve transmission through the floors and (b) paths having segments outside the buildings and involving diffraction at windows frames. The paths through the floors include the direct ray paths and the rays that are multiply reflected and transmitted at the walls and floors. These ray paths are contained entirely with in the building perimeter. The diffracted ray paths involve transmission outside the building through windows and diffraction into paths that run along side the face of the building, propagating until they reach another window, at which point the ray reenters the building at a different floor. Floors of a modern office buildings are typically constructed with precast concrete slabs, reinforced concrete or concrete poured over corrugated steel panels. UHF signals can propagate through the precast slabs and through reinforced concrete with a transmission lost at each floor. Floors constructed over a corrugated steel panels seriously limit the propagation through the floor.

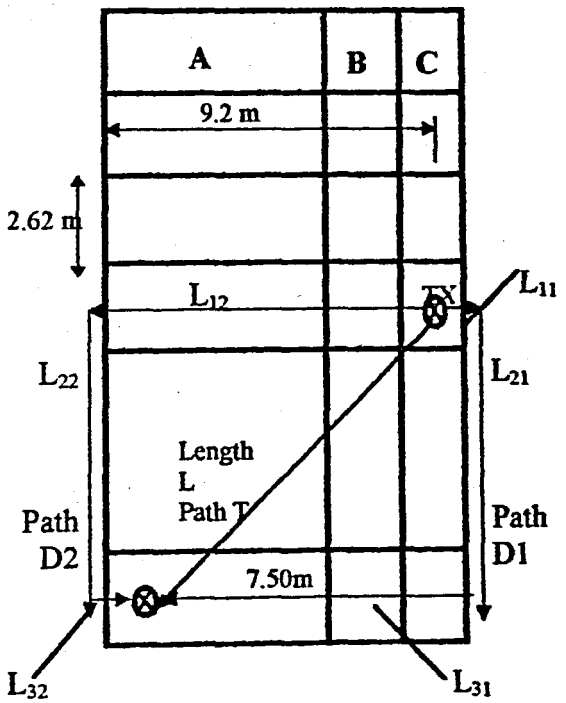

Figure 4.12. Example building for calculating the SE of the different floors

For propagation of the direct ray through floors, as indicated in by path T in Fig.4.12. the field strength reaching a receiving site is given by

$$|E|^2 = 30\frac{P_e}{L^2}\prod_m T^2_{Floor(m)}\prod_n T^2_{Wall(n)} \tag{4.27}$$

Here again P_e is the effective radiated power, and L is the direct distance between transmitting and receiving antennas. The field transmission coefficients are for the spectral transmission at floors and walls crossed by the direct ray. Such a direct ray passing through three floors and two interior walls is indicated in Fig.4.12. The signal can also reach other floors via paths that involve diffraction. Referring to paths D_1 and D_2 in Fig. 4.12. as an example, the signal can propagate horizontally from the source to windows on the outside walls on the right and left sides. Passing through the windows, the fields can then be diffracted through 90^0 by the window frame, and thereby propagate vertically along the face of the building. At windows on other floors,the field diffracts back into the building, finally reaching the receiver. The field reaching the receiver via one such diffracted path is given by. .[6]

$$|E|^2 = \frac{Z_0 P_e}{4\pi}\frac{\prod_i D^2(\alpha_i)\prod_j T^2_{Glass(j)}\prod_k T^2_{Wall(k)}}{\sum_n L_{nm}\prod_n L_{nm}} \tag{4.28}$$

where L_{nm} (n=1,2,3; m=1,2) are the lengths of the path segments for paths D_1 and D_2. $T_{Glass(m)}$ and $T_{Wall(n)}$ are the transmission coefficient through glass and through interior walls crossed by the path segments. We can present tle $L_{i,j}$ values for Figure 4.12 in a matrix form as

$$L_{ij} = \begin{bmatrix} 0.4 & 9.2 \\ 2.62\times k & 2.62\times k \\ 7.5 & 2.1 \end{bmatrix} \tag{4.29}$$

where k=number of floors

In Eq.(4.28) $D(\alpha_i)$ is the diffraction coefficient for a propagating ray bending through angle α_i. Depending on the construction of the building and window frame,

different choices may be made for the diffraction coefficient. For simplicity in investigating the relative strength of the fields associated with the direct ray and the diffraction path we make use of coefficient for an absorbing wedge, which is given by .[6]

$$D(\alpha_i)=\frac{1}{\sqrt{2\pi k}}\left[\frac{1}{2\pi+\alpha_i}-\frac{1}{\alpha_i}\right], \tag{4.30}$$

where $k=2\pi/\lambda$ is the wave number.

The numerical calculations of the direct ray and the diffraction path are obtained for the two paths. The direct ray passing through floors decreases by the square of the transmission coefficient (10 dB or more) for each additional floor. This variation, together with the $1/L^2$ dependence in Eq.4.28, results in a significant decrease from floor to floor. For diffracted paths, causes large path loss even for a single floor separating the transmitter and the receiver, but does not change from floor to floor. However the increase in the length of the vertical path segment L_{2m} (m=1,2) in going from floor to floor will cause a small decrease in the diffracted path wave. Thus when propagation takes place through the floors the signal will decrease rapidly with the number of floors separating the transmitter and the receiver. On the other hand, if propagation occurs via diffracted paths the signal will small even for the separation by a single floor but will decrease more slowly with increase separation. Hence in buildings with reinforced or precast concrete floors the signal of the diffracted path is larger than that of the direct ray. For buildings with only corrugated steel floors propagation through the floors is not possible and the signal will reach other floors via diffracted paths.

The multilayer model results are little differed from resultts of Ref.[6] studies. It can be seen in Figure 4.13 and 4.14 that direct ray path decrease slover than the other methods. But the main characteristics of both methods are same. Therefore multilayer structure can be used for modelling a building.

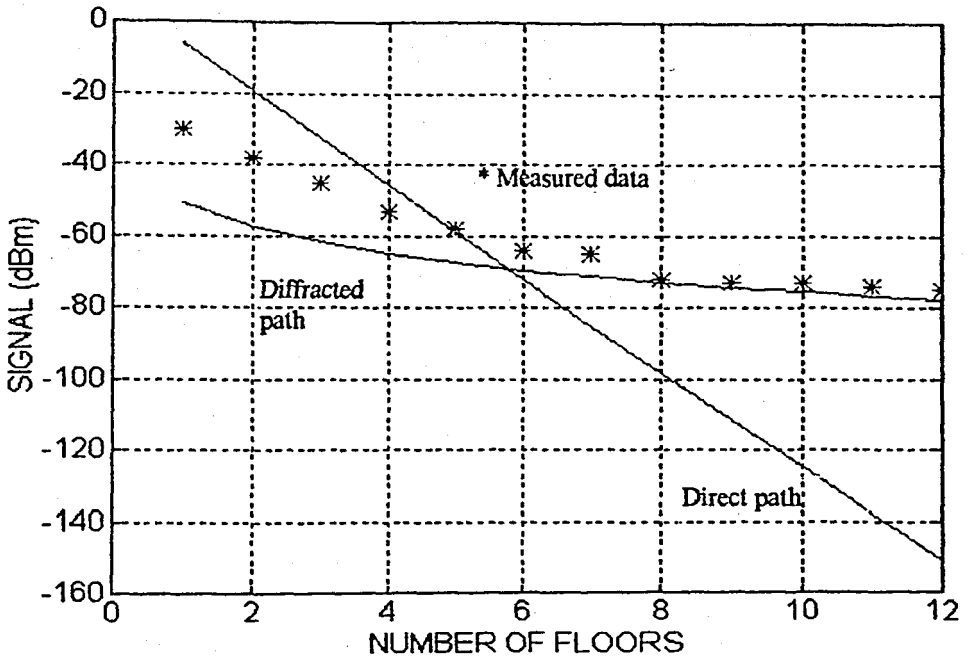

Figure 4.13 Results for parameters given in the paper [6]

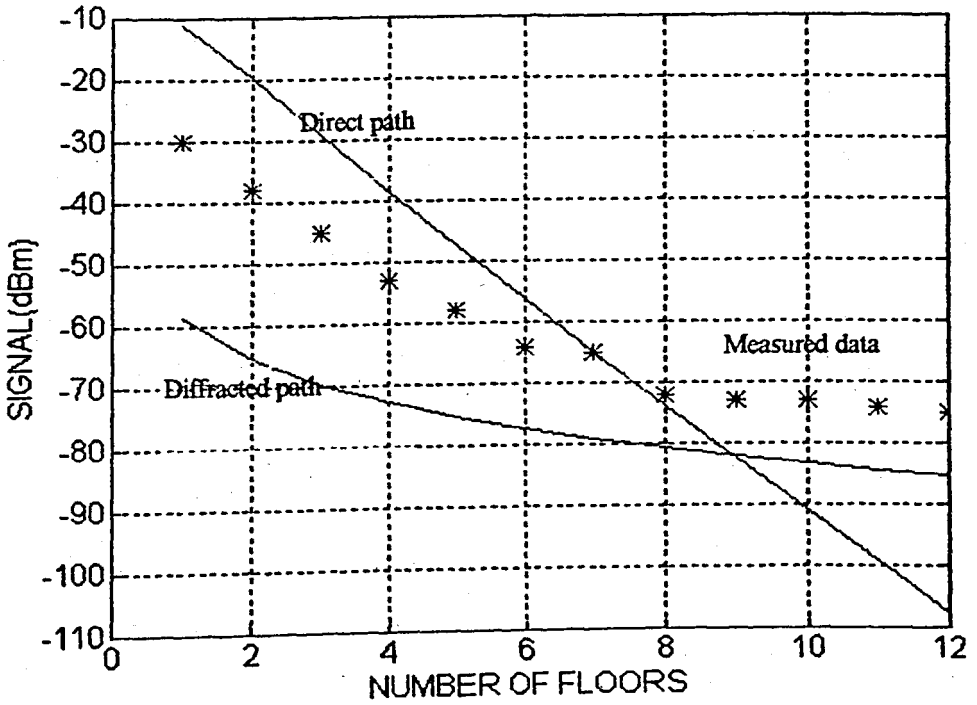

Figure 4.14 Results for parameters calculated in the multilayer program

5. MEASUREMENTS

5.1. Application to the Building of Interest: TÜBİTAK MRC Electronic Department

In this section multilayer structures were applied to the building for the same and different floors. Propagation loss measurements were done in the first and second floors of TÜBİTAK Marmara Research Center Building. The structure of each floor and the placement of offices are the same. Each floor is divided by a corridor. 70 per cent of the outside walls of the offices are composed of glasses. Walls are concrete. Doors were made of wood, but upper half of them is glass.

Transmitter antenna was placed in the second floor . The height of it from the office floor was 120 cm. Because of acuistic drop ceiling the distance between the floors is 76 cm. The receiver antenna was placed in the first and the second floor offices of the building. Its height was 112 cm.

Figure 5.15. gives the floor plan for "in the same floor" measurements, Figure 5.16. gives the floor plan for "different floor" measurements while Figure 5.17. is the setup for "different floor" measurements.

5.2. Automated Measurement System

The traditional measurement systems do not allow us to scan a particular frequency range. In order to examine more than one frequency, the synchronization between transmiter and receiver site must be provided. Therefore several researchers have dealt with this problem.

In this thesis, a synchronous test system has been used for the attenuation measuremets of the building through the rooms in the same floor. Test setup is given in Fig.5.1. Properties of devices used during the measurements are listed in table 5.1.

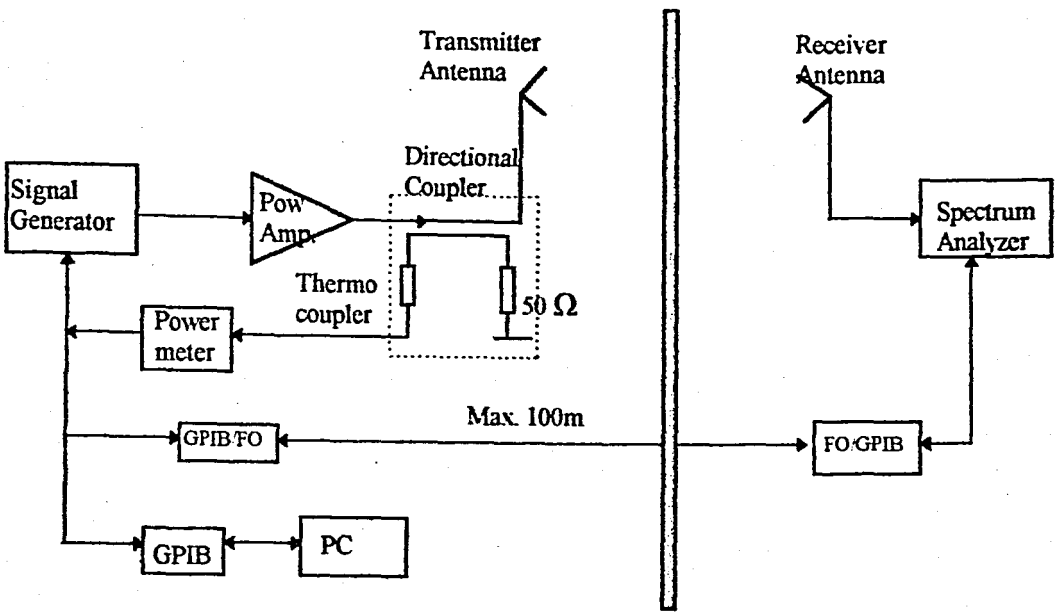

Figure 5.1. Automated mesurement setup

5.2.1 Description of the Measurement

The measurement setup shown in Fig.5.1. can be used to measure the shielding effectiveness of the building. This method allows us measuring of any building automatically by using the IEEE 488 bus with GPIB (General Purpose Interface Board).

Measurement system has an userinterface that start frequncy, stop frequency, number of steps and transmitted power values can be selected from its menus. In this study the limits for the frequency range were chosen 200 MHz - 1000 MHz respestively and the number of steps is 100. Using automation system all devices are reset then signal is began to generate. For the single floor the transmitted power was 0.5 W. In order to obtain this constant power value a feed back is used to control output of the power amplifier. In the interval of ±0.04 tolerance the transmitted power is checked by powermeters in the CVI program.

The transmitter antenna is shown in Fig 5.2. Radiation pattern of conical log spiral antenna is given in Appendix A. Figure 5.3. shows the power meter, signal generator and the power amplifier which are installed in the rack. Figure 5.4 and 5.5. show the spectrum analyzer and receiver antenna used in receiver site of the measurement system. Communication between signal generator and spectrum analyzer is obtained by the fiber optic cable with GPIB extender.

The difference beetween these transmitted and received signals in dB gives us the shielding effectiveness of this barrier.

Table 5.1. List of the measurement devices

Device	Model	Frequency Range	Serial No.
Signal Generator	Rohde&Schwarz SMY01	9kHz-1040MHz	1062.5502.11
Spectrum Analyzer	HP 8591E	9kHz-1.8 GHz	3647U02/95
Receiver Antenna	MEB Reference Source VSQ	30MHz-1GHz	12001
Transmitter Antenna	Conical. Log Spiral Antenna HUF-Z4	200-1000MHz	837.2210.52
Power Amplifier	Amplifier Research 50W1000A		1006800-501
Power Meter	Rohde&Schwarz NRVS		1020.1809.02
Directional Coupler	MEB	0.01-1000MHz	
PC	Tulip Notebook		FT6000A

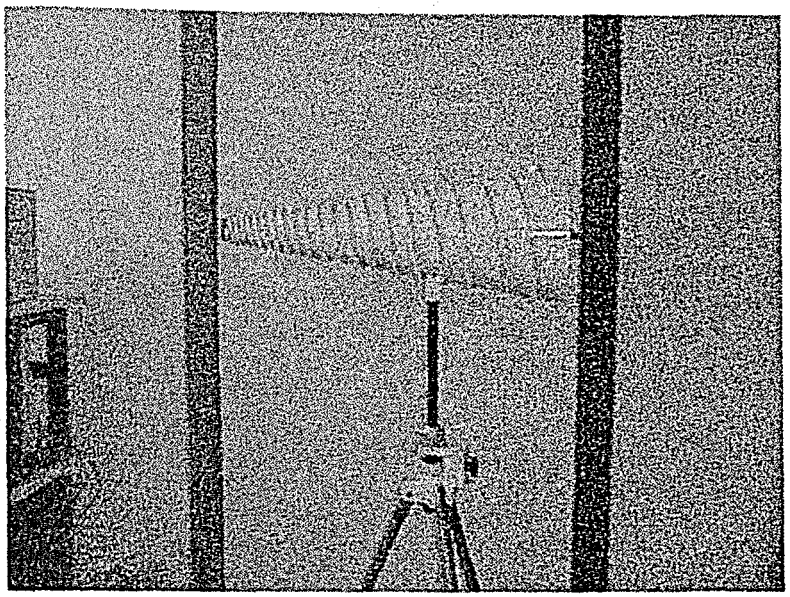

Figure 5.2. Conical Log. Spiral Antenna at the Transmitter Site

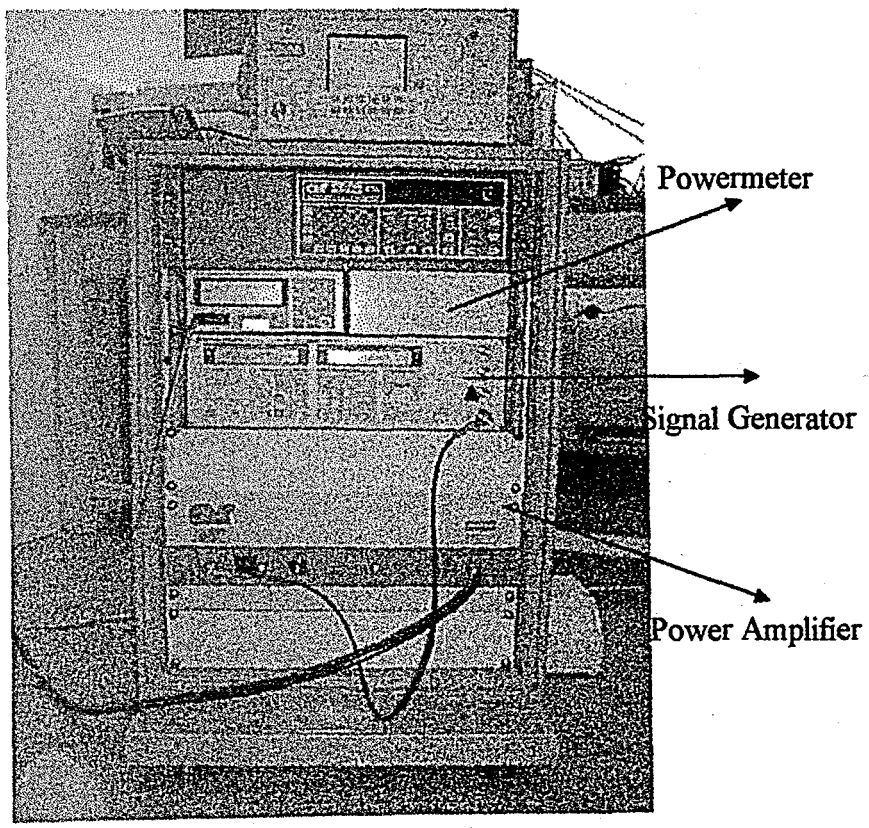

Figure 5.3. The Transmitter System in Use

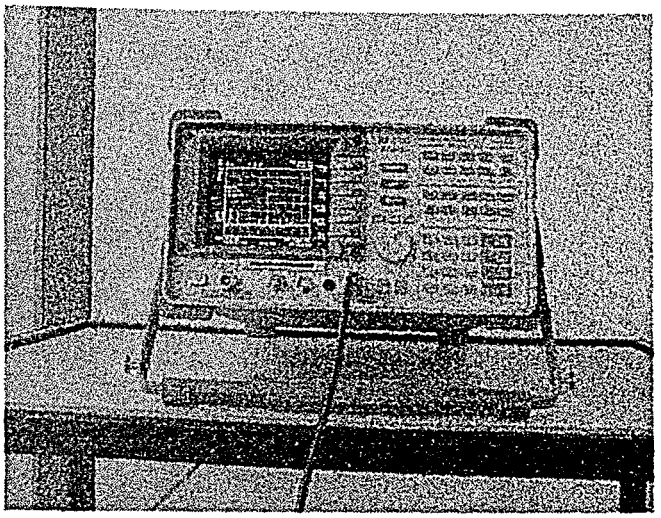

Figure 5.4. Spectrum Analyzer

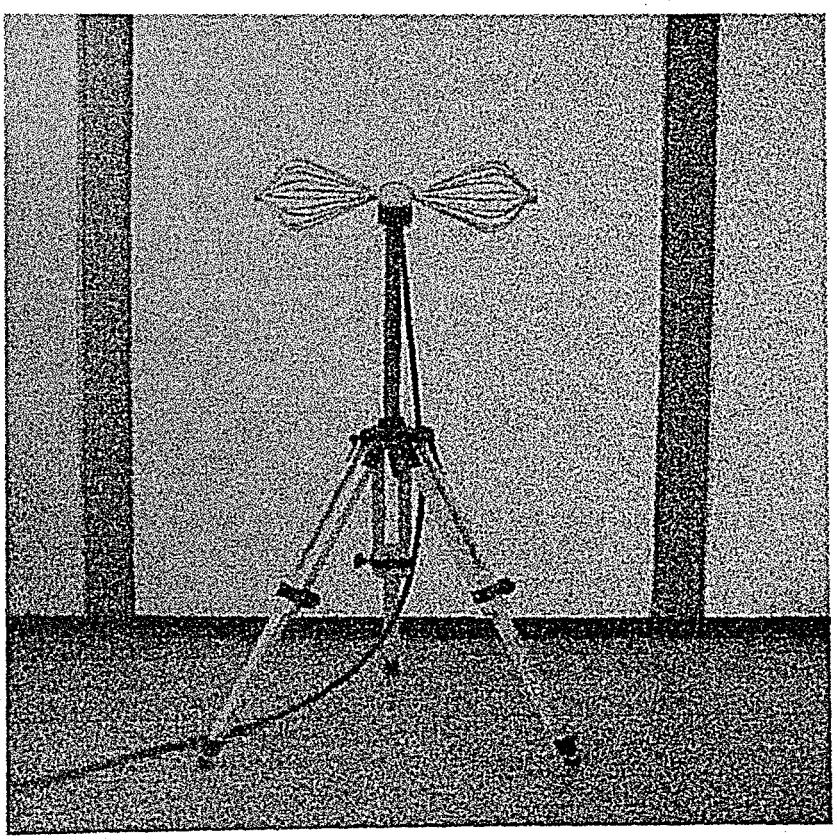

Figure 5.5. Biconical Receiver Antenna

5.3. Measured and Calculated Results for Single Floor

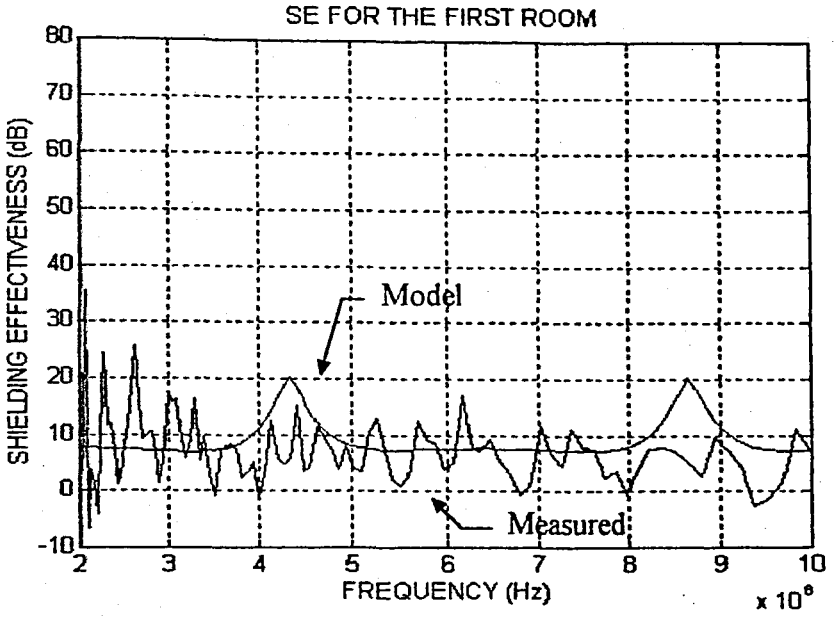

Figure 5.6. Results for the first room.

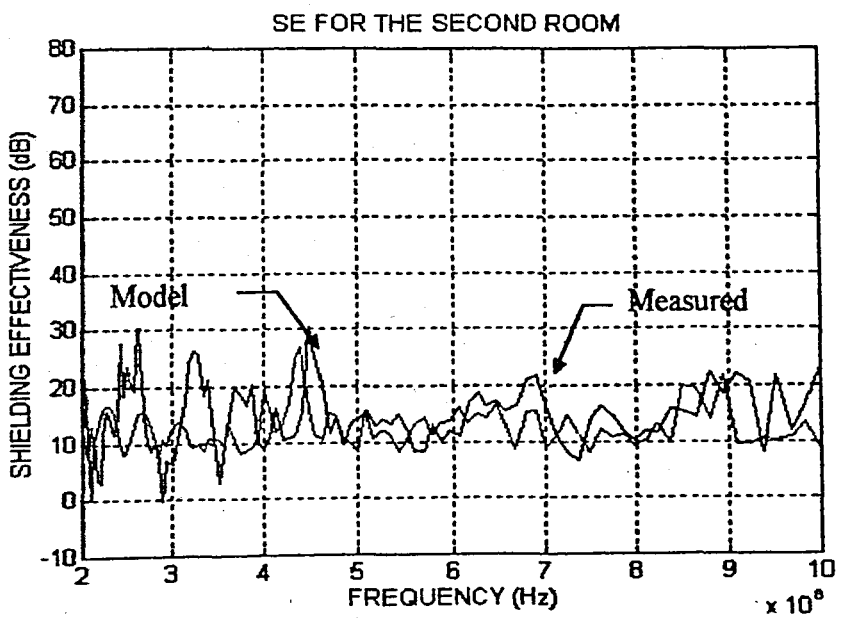

Figure 5.7. Results for the second room.

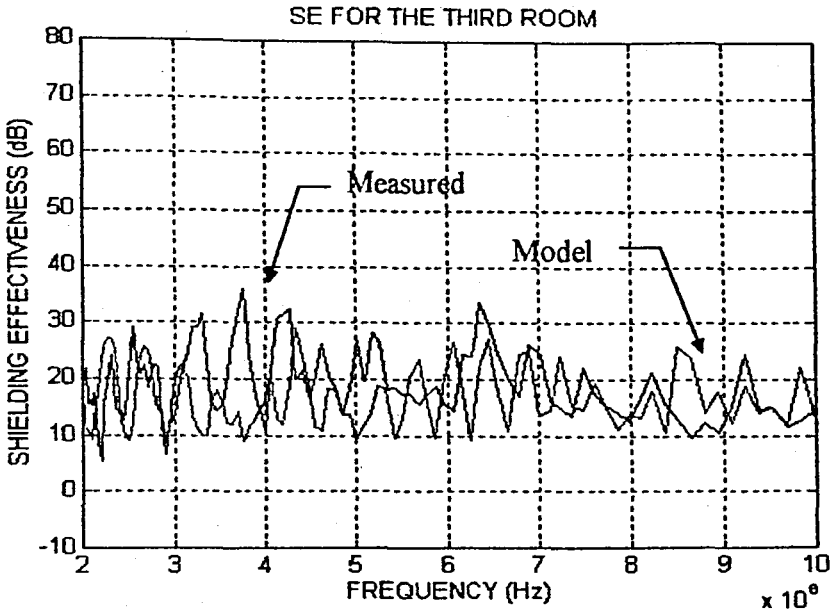

Figure 5.8. Results for the third room.

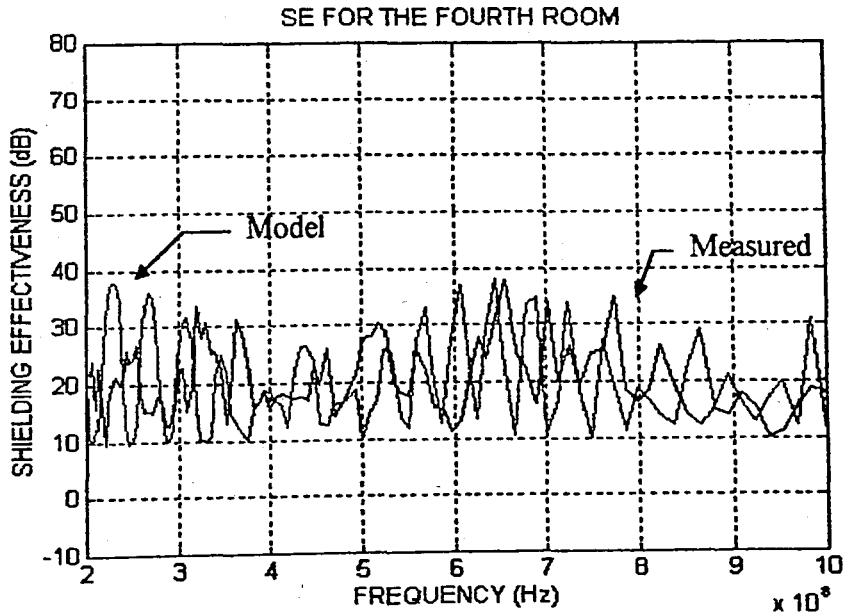

Figure 5.9. Results for the fourth room.

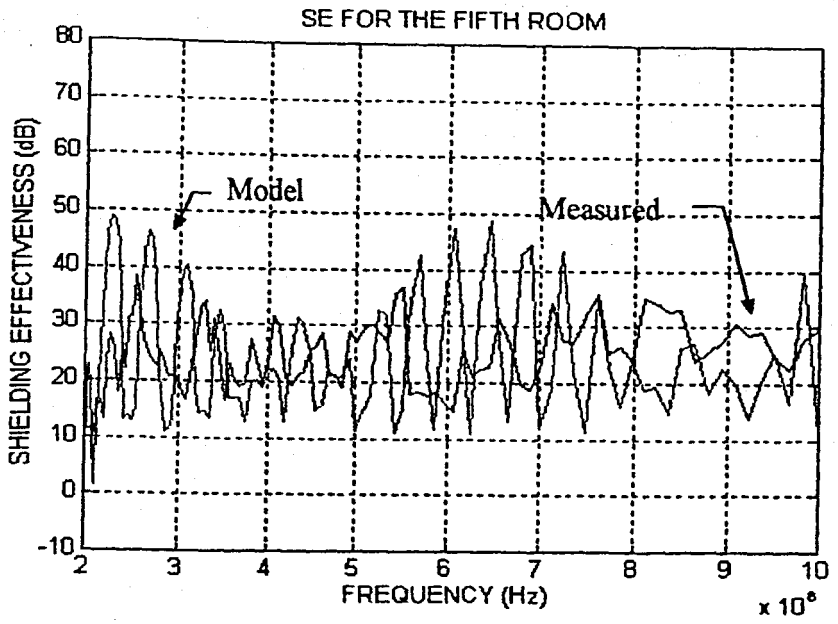

Figure 5.10. Results for the fifth room.

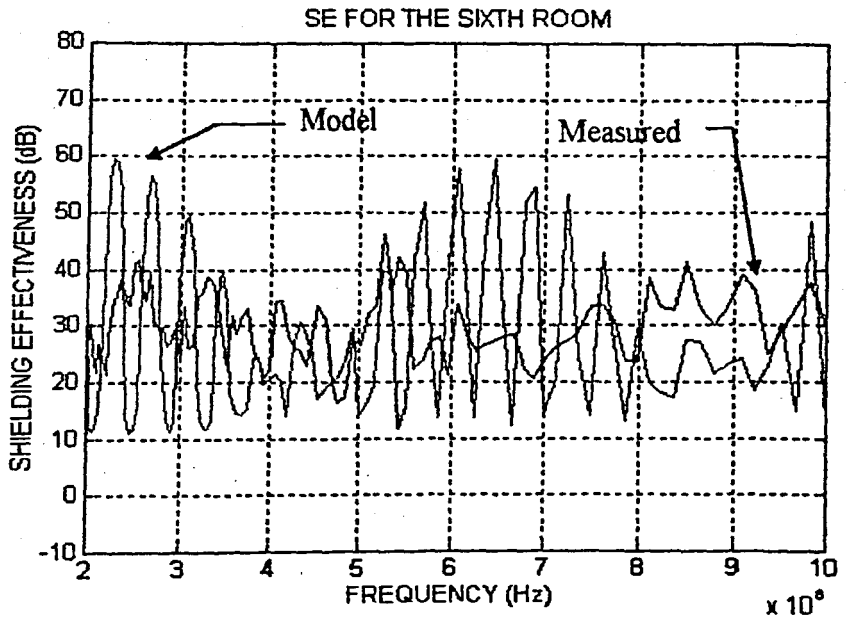

Figure 5.11. Results for the sixth room.

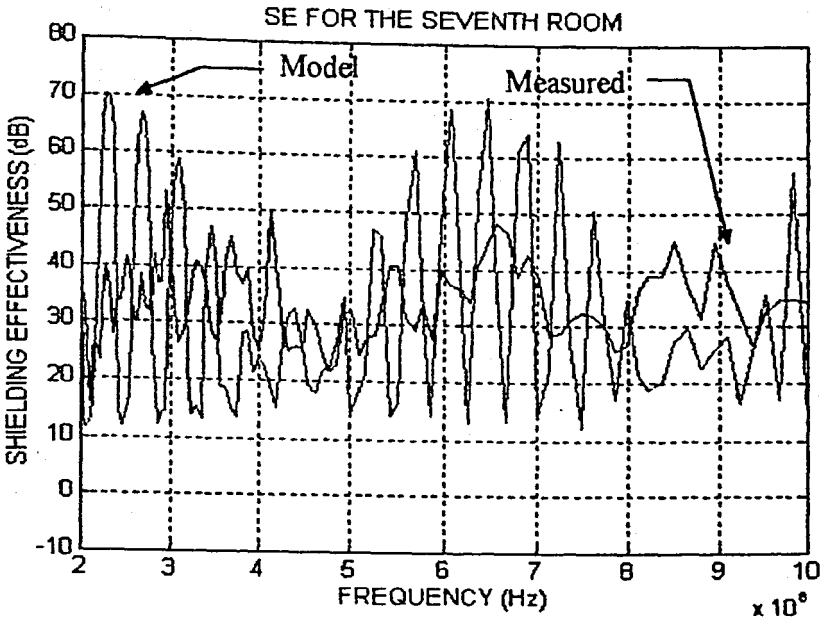

Figure 5.12. Results for the seventh room.

Figure 5.6-5.12 show the calculated and measured results of the seven rooms on the same floor for 200 MHz-1000 MHz. Both of these results were obtained for 100 frequency step. The distance between receiver and transmitter seems to have significant effects on calculated results But the several factors effect the wave propagation such as reflection from the transmission media (ceiling, walls, floor, furniture etc.) Therefore some difference may occur between calculated and measured results although these effects were considered in the modeling.

The peaks seen on the measured graph are results of ambient radiation which are inherent in the propagation media because of the broadcasting radio stations, GSM, TV channels.

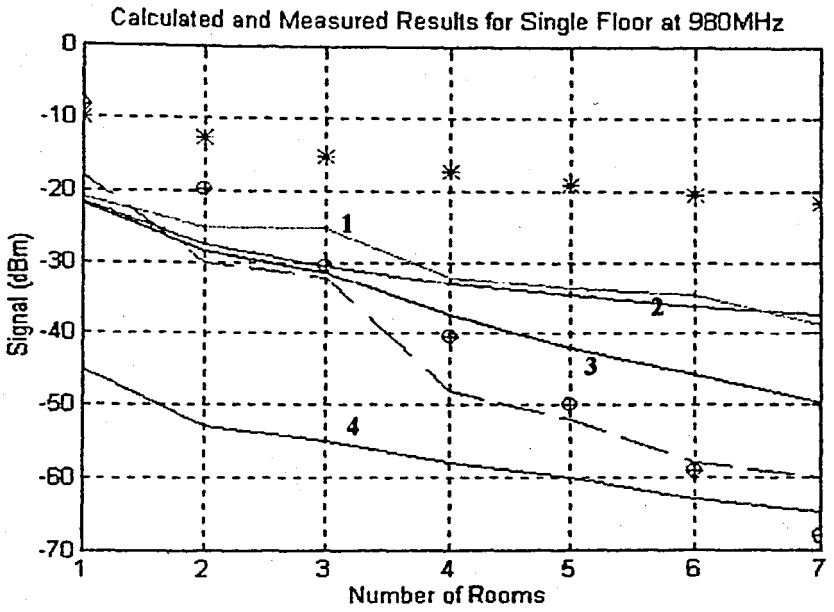

Figure 5.13 Individual Effects on the Received Signal

—: Measured Signal

⊕: Direct path

*: Reflected wave from wall

1: Reflected wave from ceiling

2: Reflected wave from floor

3:Calculated Signal

4: Diffracted path

It is difficult to distinguish effects of the received waves individually for the direct ray or reflected waves from the walls, floors or ceiling on the total received signal in a frequency range. Therefore if a received signal were examined at a single frequency the attenuation through the rooms and individual effects could be seen clearly. From the Eq.(4.26) we can calculate the all received signal. The results of this investigation are shown in Fig. 5.13.

At 980 MHz on the same floor diffracted waves have no significant effect on the total received signal except for the seventh room. While for the first three rooms reflection from floor and ceiling have significant effects on total signal, for the other rooms the directly transmitted waves are closer to the measured signal than the other paths.

But these results are only valid at 980 MHz. Depending on the frequency, wavelength, dimensions of the rooms and distance between transmitter and receiver antenna results will change.

5.4 Measured and Calculated Results for One Floor Down

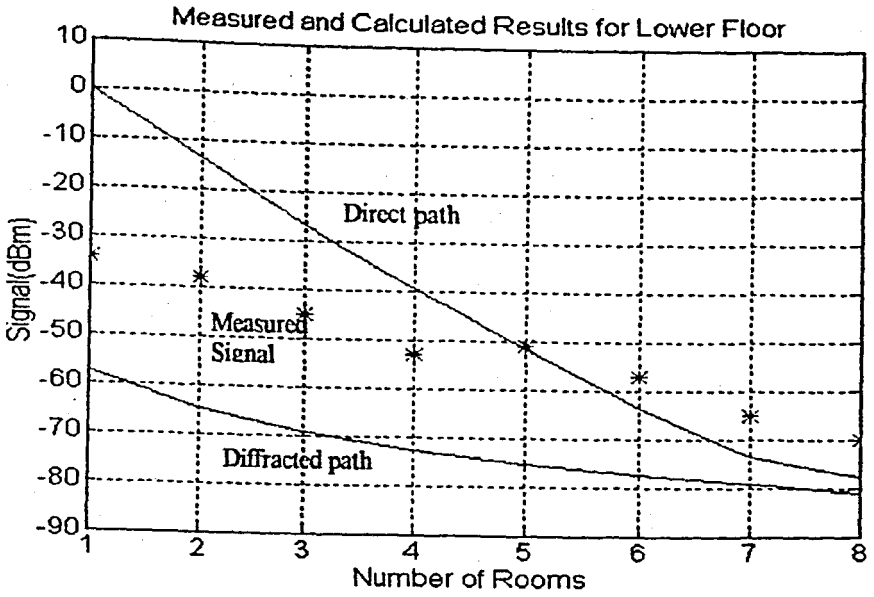

Figure 5.14. Results for Lower Floor

Becaues of the installation difficulties of the measurement system, frequency scanning was not achieved. However at a single frequency of 980 MHz different floors measurements could be carried out. The calculated and measured signal are shown in Figure 5.14.

SE calculation inside the building for different floors does not like in the same floor. Corresponding two ways: (1) direct path and (2)diffracted path show different attenuation characteristics through floors. From the Eq. 4.27 and Eq. 4.28 we can easily calculate the direct and diffracted path effects on the receive signal.

The case where the transmitter and the receiver antennas are located on the different floors it is expected that the direct ray has more effect for close distance while diffracted waves have more effects for large seperation distances of the antennas. This valid for the isotropic antennas which are equally polarized for all dimensions. In this study directive antennas have been used and the main lobes of their radiation patterns were not aligned to see each other . So for the first two rooms the measured signal is not closer to the calculated direct signal.

Diffracted ray path for the one floor down are not effective because of the antenna radiation pattern and the building characteristic.

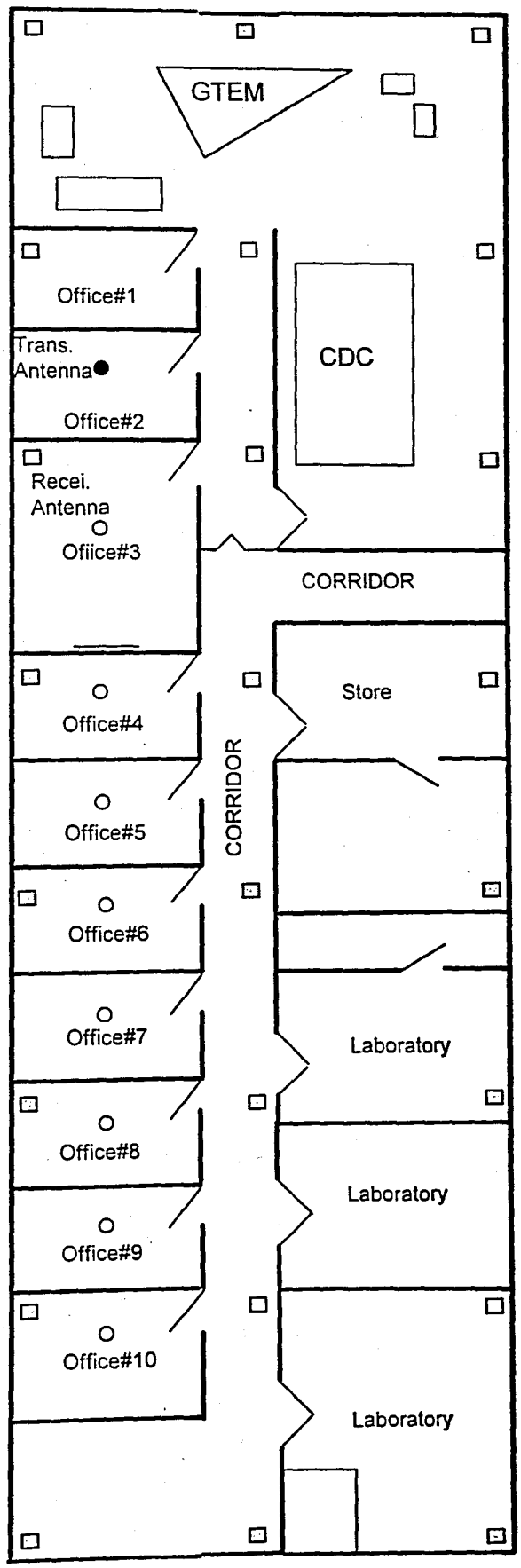

Figure 5.15. Floor plan for in the same floor measurement.

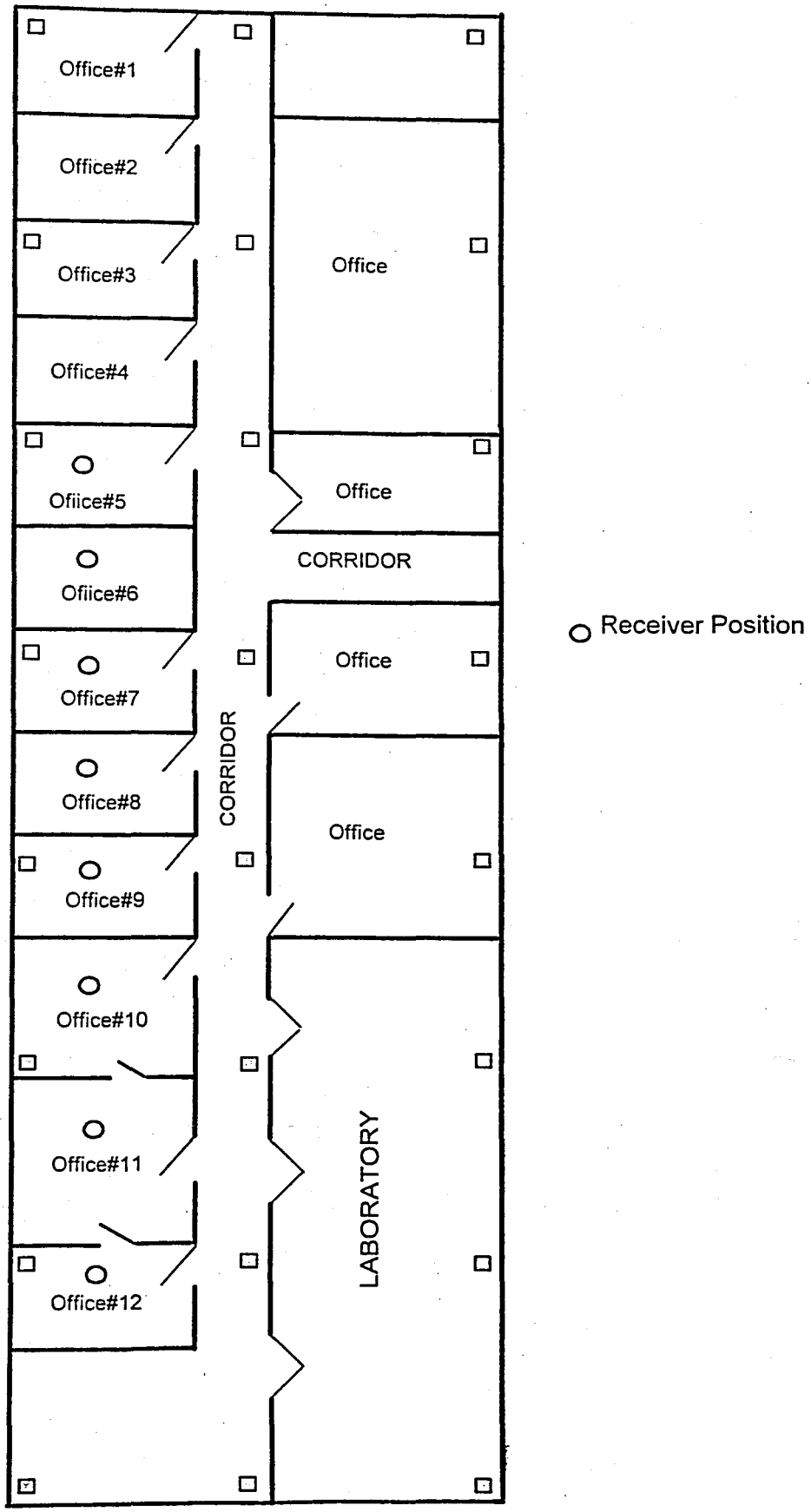

Figure 5.16. Floor plan for different floor measurement.

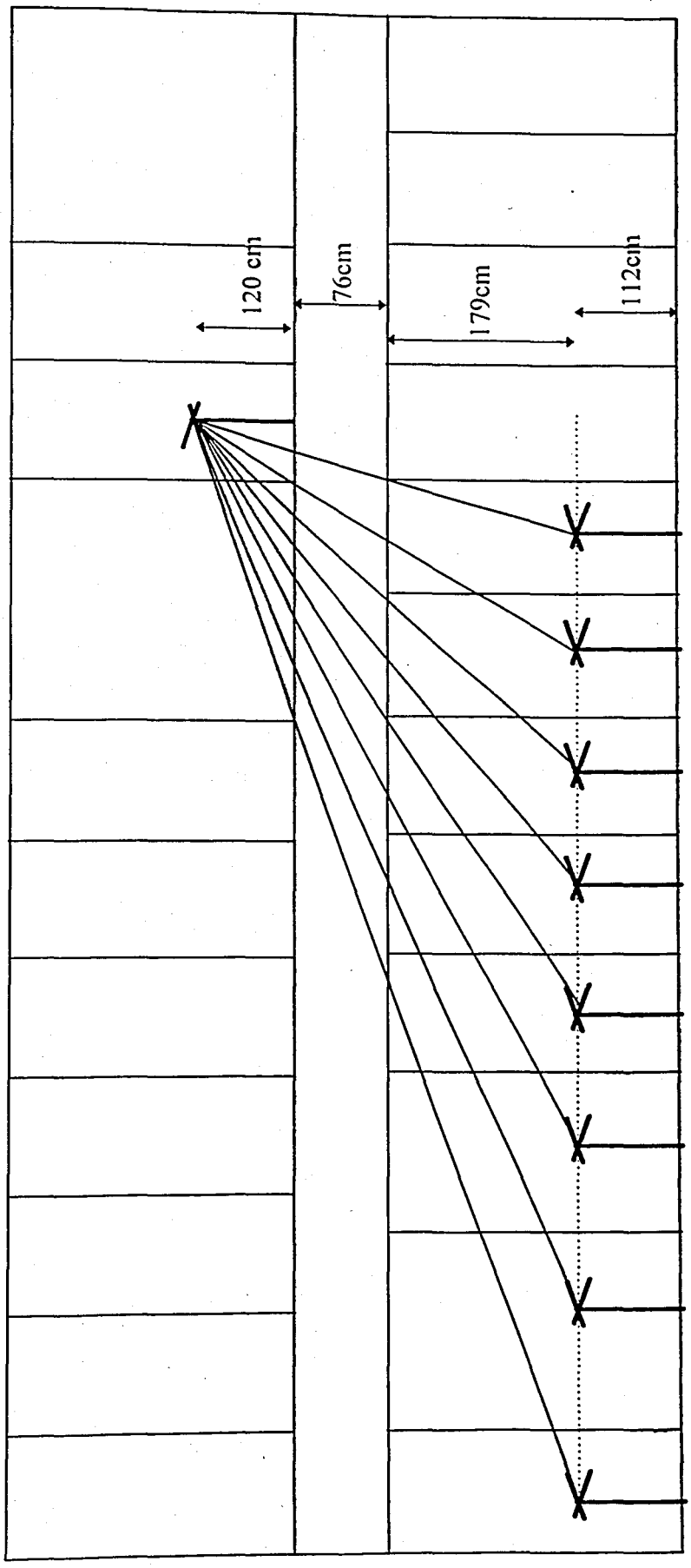

Figure 5.17. Setup for different floor measurement

6. SHIELDING EFFECTIVENESS MEASUREMENT METHODS

6.1. Standard: MIL-STD 285

MIL-STD-285 (dated June 1956) is entitled "Attenuation Measurements for Enclosures, Electromagnetic Shielding, for Electronic Test Purposes, Method of. " This standard covers a method of measuring the attenuation characteristic of electromagnetic shielding enclosures used for electronic test purposes over the frequency range 100 kHz to 10 GHz. It consist of three measurement methods for different freqency range. [13]

1. Measurement of attenuation low impedance (magnetic) fields :
   Test frequency :One frequency in the 150-200kHz range
   Transmitting and receiving antennas are loop antennas of 30cm diameter
2. Measurement of attenuation to high impedance (electric) fields:
   Test frequency : 200 kHz, 1 MHz, 18 MHz
   Transmitting and receiving antennas are rod antennas
3. Measurement of attenuation to plane waves :
   Test frequency : 400 MHz
   Transmitting and receiving antennas are dipole antennas

In this method the shield is illumunated by a signal source, power amplifier(if needed) and transmitting antenna. A receiving antenna is placed on the other side of shield and the resulting electromagnetic field is then measured using a detection system consisting of an EMI receiver or spectrum analyzer and attenuators and /or preamplifiers (if needed) Fig. 6.1. Two readings are made, one with and one without the shield barrier in place. The SE is defined as the adjustment (increase) of the dB attenuation setting on the receiver (or the source) which produces the same reference reading when the shield wall is removed, without changing the position of the antennas. The rationale is that precision attenuators give better accuracy and repeatability than a receiver display. However, with the introduction of modern receivers with tracking generators, readout and operator errors have been eliminated by digital data processing.

This frequency limitation was inherent in the suggested measurement equipment which has long since become obsolete. Because the techniques for sound people have used MIL-STD 285 for over 35 year, but have modified its frequency range and test equipment to meet their needs. Now it appears that military is in the process of withdrawing MIL-STD 285 to replace it with IEEE Std 299-1991 which was developed specifically for that purpose.

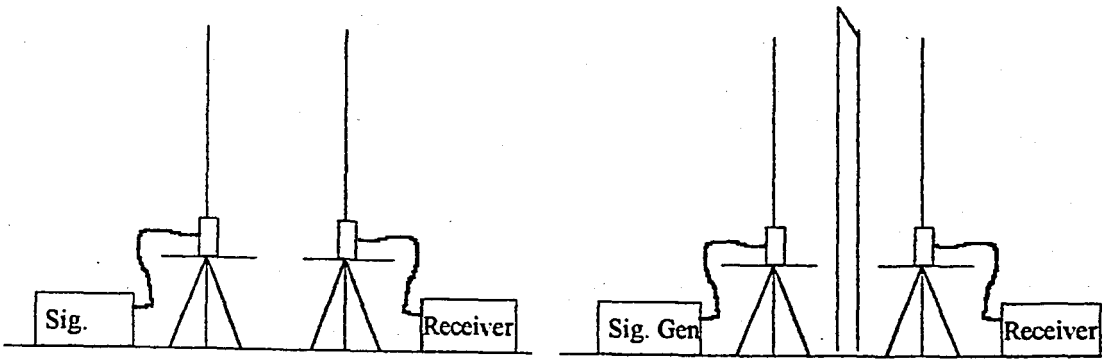

Figure 6.1 -MIL-STD-285 General Test Setup For Field Attenuation Measurements

6.2. IEEE 299-1991

IEEE Standard Method for Measuring the Effectiveness of Electromagnetic Shielding Enclosures

This standard provides uniform measurement procedures and estimation techniques for determining the effectiveness of room size, high performance electromagnetic (EM) shielding enclosures at frequencies from 14 kHz to 18 GHz (Extendible to 50 Hz and 100 GHz, respectively). These procedures may be used throughout these range (except for some excluded frequencies) although certain frequencies are required. [14]

The measurement procedures determine the EM shielding performance of various type of enclosures including these characteristic *1) Configurations*:single shield or double shield , *2) Consruction*:demountable (bolted), fixed-seam (welded, brazed or soldered),

integral with building *3) Materials*:steel plate, copper or aluminum sheets; screening; hardware cloth; metal foil

6.2.1. General Procedures

This section specifies the antennas for the measurements and describes a required preliminary search for locations of poor performance. The preliminary procedures include checking the field strength meter shielding, removing non essential equipment from the shielded enclosure. A shielded enclosure leak detector may be used for the preliminary scan. Figure. 6.2. The basic measurement procedure consist of placing a source outside and a detector inside of the enclosure to be evaluated and measuring over all walls, containing seams, doors and penetrations.

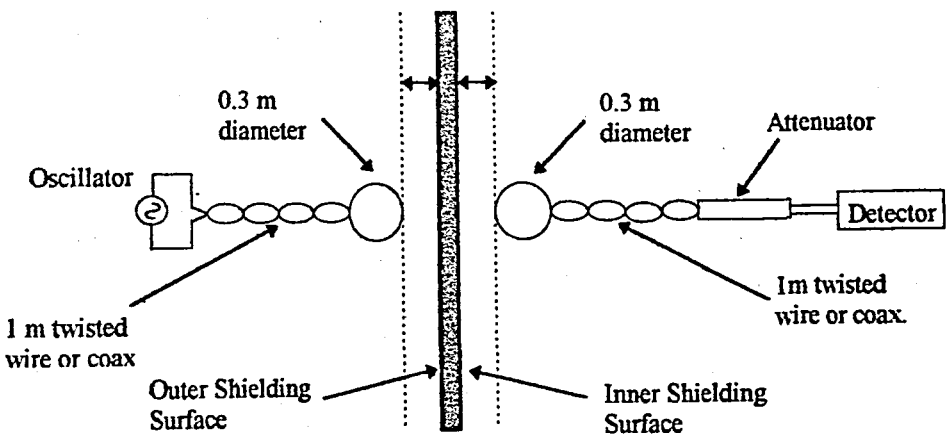

Figure 6.2. Attenuation measurement of low impedance magnetic field.

6.2.2. Detailed Procedures

The detailed procedures are divided into three separate frequency range given in Table 6.1.and for each range the standard discusses test equipment, test frequencies

preliminary procedures, free field calibration measurement procedures and determining the shielding effectiveness.

Table 6.1. Standard Measurement Frequencies

Standard Frequency	Measurement type	Antenna
Low range 14-16 kHz 140-160 kHz 14-16 MHz	H field	Small loop
Midrange 300-400 MHz 850-1000 MHz	E Field	Dipole
High Range 8.5-10.5 GHz 16-18 GHz	Plane wave	Horn

You can find detailed information about the measurements in Ref [14]

6.3. Comparison of the MIL-STD 285 and IEEE Std. 299

IEEE Std. 299 covers the complete range of frequencies for which modern room size enclosures are used, namely 14kHz to 18GHz with extensions down to 50 Hz and up to 100 GHz. MIL-STD 285 only covered 100 kHz to 10 GHz but had no test near the 10 GHz. IEEE Std. 299 thus standardizes measurements which people have been making for many years outside the frequency range covered by MIL-STD 285.

IEEE Std. 299 uses magnetic shielding effectiveness measurements alone in the lower frequencies where measurements are made entirely in the near field. This is an improvement because it eliminates trouble some electric field measurements using rod (monopole) antennas. The electric field measurements were very sensitive to their surroundings and were usually not repeatable within a resonable tolerance. The magnetic field measurements on the other hand are not very sensitive to their surroundings and they are stable and usually repeatable. Furthermore the electric field measurements realy proved nothing about the shielded enclosure that could not be found out by magnetic field measurements if a seam or penetration is sealed well for electric field too. By eliminating the

electric field measurements below 20 MHz, IEEE Std. 299 has reduced the measurements burden while improwing measurements reliability.

IEEE Std. 299 takes the economical approache of first searching for locations of leakage in the enclosure and correcting those problem before spending a large amount of time and effort on a full-blown shielding effectiveness test. MIL-STD 285 did not suggest this kind of approaches. IEEE 299 suggests simple, modern instrumentation, leaving the user of the standard the freedom to select specific instrumentation. It gives a great deal of useful information in its appendices to help the user to better understand the test and the reasons for them. MIL-STD 285 didn't supply this kind of information. Finally IEEE 299 requires a competent report of the tests to assure their quality of the shielded enclosure. [15]

6.4. Automated Measurement of MIL-STD 285

The first question that comes to mind at this point is why bother to automate at all. For standard welded or modular shielded enclosures the manual methods in wide spread used are quite adequate to characterize the performance of the shield. The shielding effectiveness is such that testing over a small number of spot frequencies will adequately define the performance over the entire frequency range of interest.

This is not the case where nontraditional shielding technologies are used (such as composites, sprays, etc.) or when it is desired to measure the attenuation of real case building at any frequency range. Any task that is done repetitively is a candidate for automation. The collection, computation and plotting of the large number of points required to charactize a non traditional shield at any given test location is a pirime candidate for automation. The advantages of improved accuracy and productivity are obvious.

There are two basic approaches to performing shielding effectiveness measurements over a continuous range of frequencies: asynchronous and synchronous testing. In asynchronous testing the signal source is continuously swept over tile range of interest. The detection system (EMI receiver or spectrum analyzer) is also swept over tile same range. Both tile source and tile detection system are swept independently. The peak hold function of the detection system is used and when both are at tile same frequency at the same time, a

measurement is taken. Over a period of time a scan is "built up" and measurements are taken at all frequencies. This technique can be implemented using readily available commercial test equipment without any software development. [16]

Often a spectrum analyzer that has an X-Y function and plotter driver firmware is used. Broadband EMI antennas such as loops, vertical rods, biconical dipoles and log conical spirals are used. This reduces the number of different setups required to cover the entire frequency range of interest. Any continuous wave (CW) generator capable of performing frequency sweeps over the antenna frequency range is suitable.

The main advantage of this method is in its simplicity, but the time required to perform a sweep is a potential disadvantage. If the required dynamic range is high (for example 110 dB), then narrow detection bandwidths will be required. This means slower sweep times for both the detection system and the source to be certain that the resulting measurements are accurate. Since multiple sweeps are required to ensure that measurements are taken at all frequencies, considerable time will be required to perform the measurements. In order to cover the 200 MHz to 1 GHz frequency range using a 10 kHz bandwith, a test time of over 10 hours per test point is required.

In synchronous testing both the signal source and detection system are swept through the frequency range of interest once, ensuring that the source and detection system are always at the same frequency. This increases the test setup complexity but can reduce test times dramaticaly. A 200 MHz to 1 GHz sweep using a 10 kHz bandwidth can be performed in about 2 hours.

The simplest way of implementing this method is to use a spectrum analyzer with a tracking generator as the signal source. A penetration of the shield will be required to bring the signal to the other side of the shield. In some cases a power amplifier will also be required to achieve the required dynamic range.

Another method is to use an instrument controller (i.e., computer) to send the necessary commands to both the signal source and the spectrum analyzer. Depending on the instrumentation selected, communications between the instruments may be accomplished using RS-232 or IEEE-488 links. Either wire or fiber optic lines may be used as a communications medium. Depending on configuration, a penetration of the shield is required to carry either communications or the RF signal.

In this thesis a synchronous test system is used for measuremet the attenuation of the building through the rooms in the same floor. Test setup is given in Fig. 5.1. Equipment used during the measurement are shown in Table 5.1.

6.5. SE Measurements of Shielded Enclosures

The CDC used for some EMC tests is a shielded enclosure made of galvanized steel whose dimensions are 7 x 3.04 x 3.12 (L x H x W). The inner walls, ceiling and floor of the enclosure are covered with ferrite tiles to make it anechoic as seen in Figure 6.3.

Before the ferrite tiles were installed the magnetic shielding effectiveness of the enclosure was measured using magnetic loops. The results are given in Table 6.3-6.6.

The ambient levels of the chamber were measured before and after the installation of the tiles. The ambient levels of the location outside the chamber was also measured. The results are given in Figures 6.4-6.13

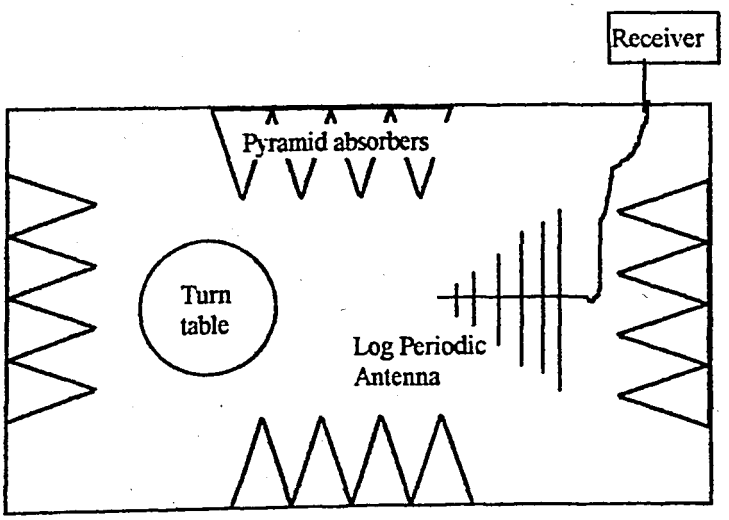

Figure 6.3. Measurement setup after the absorber installation

6.5.1. Noise Level of the CDC and Ambient

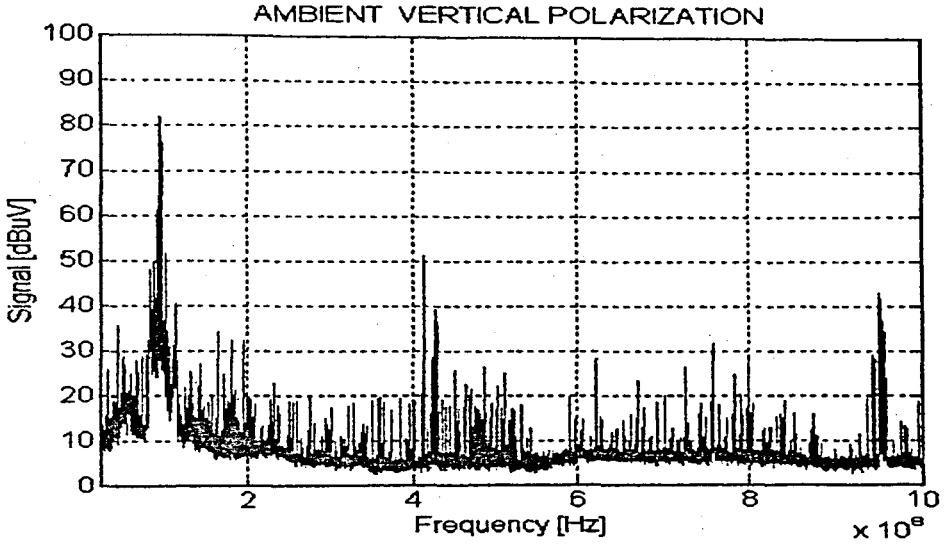

Figure 6.4. Ambient Level Outside of the Chamber Vertical Polarization

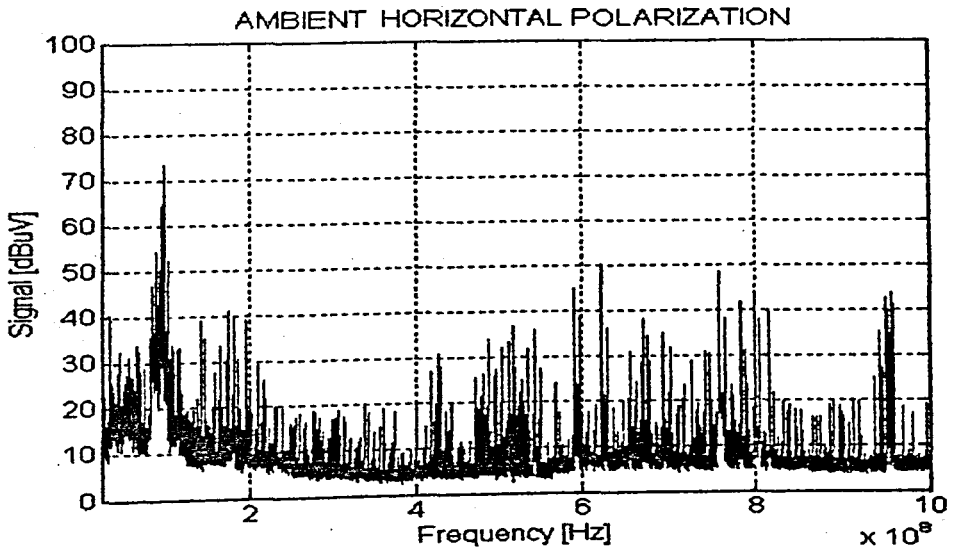

Figure 6.5. Ambient Level Outside of the Chamber Horizontal Polarization

Figure 6.4. and 6.5. show the ambient level outside of the CDC for vertical and horizontal polarization respectively. FM radios, TV channels and the GSM signals cause peak level in the spectrum.

6.5.2. Measurements Results Before Absorbers Installation

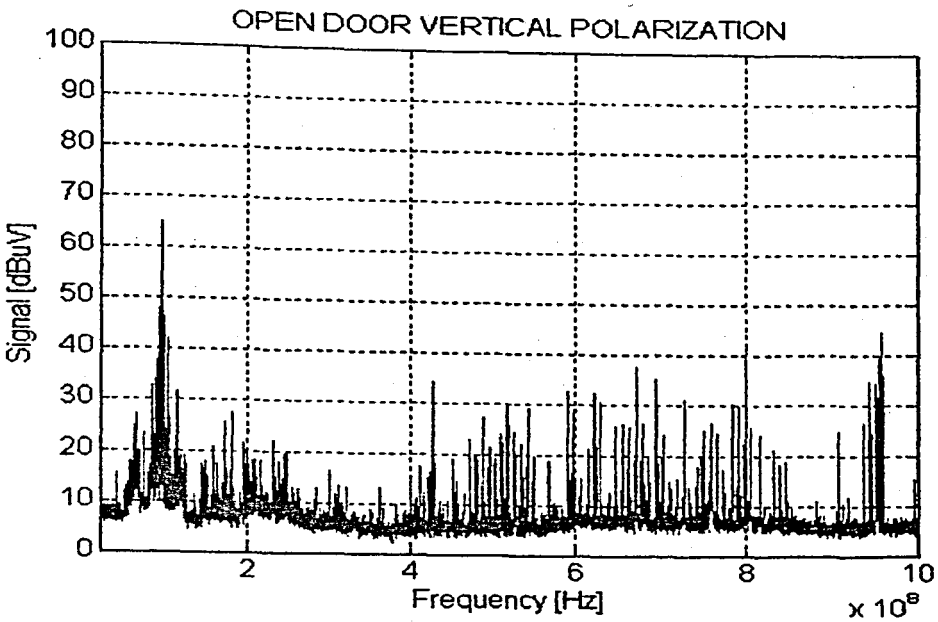

Figure 6.6. Before Absorbers Installation Open Door Vertical Polarization

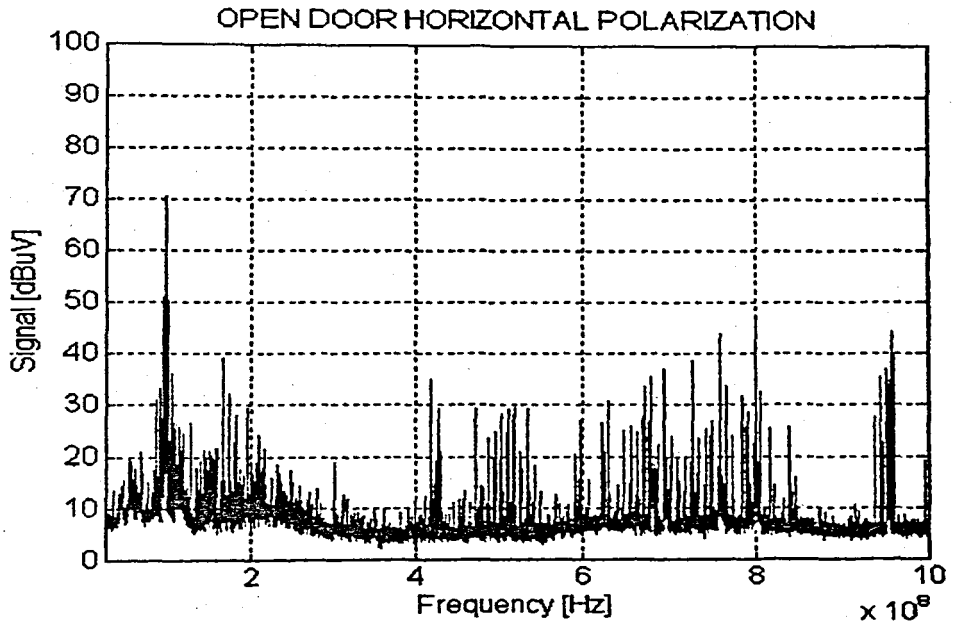

Figure 6.7. Before Absorbers Installation Open Door Horizontal Polarization

Figure 6.6. and 6.7. show the case of the ambient signal inside the CDC but but the door is not closed. There is a little attenuation because of the CDC wall .

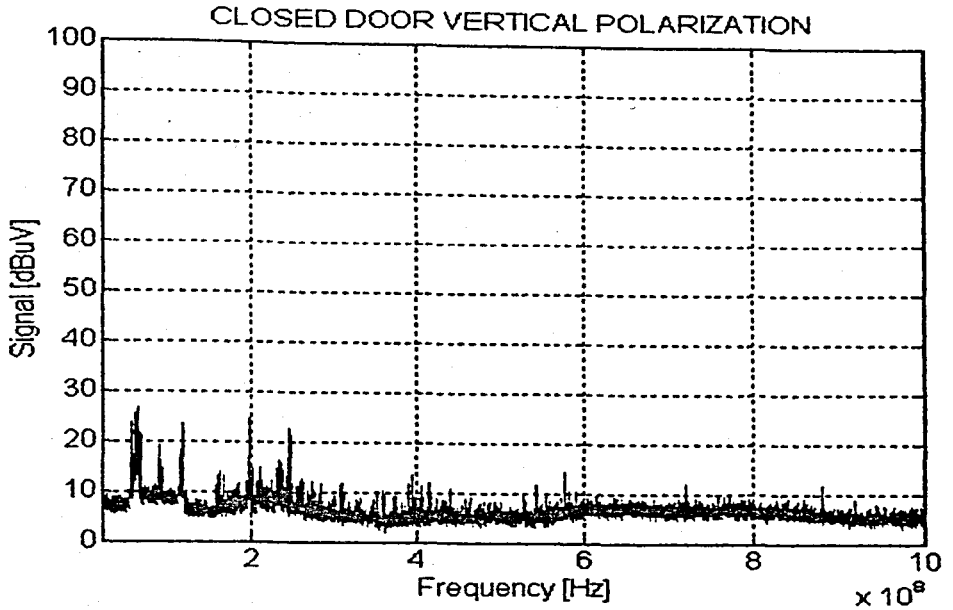

Figure 6.8. Before Absorbers Installation Closed Door Vertical Polarization

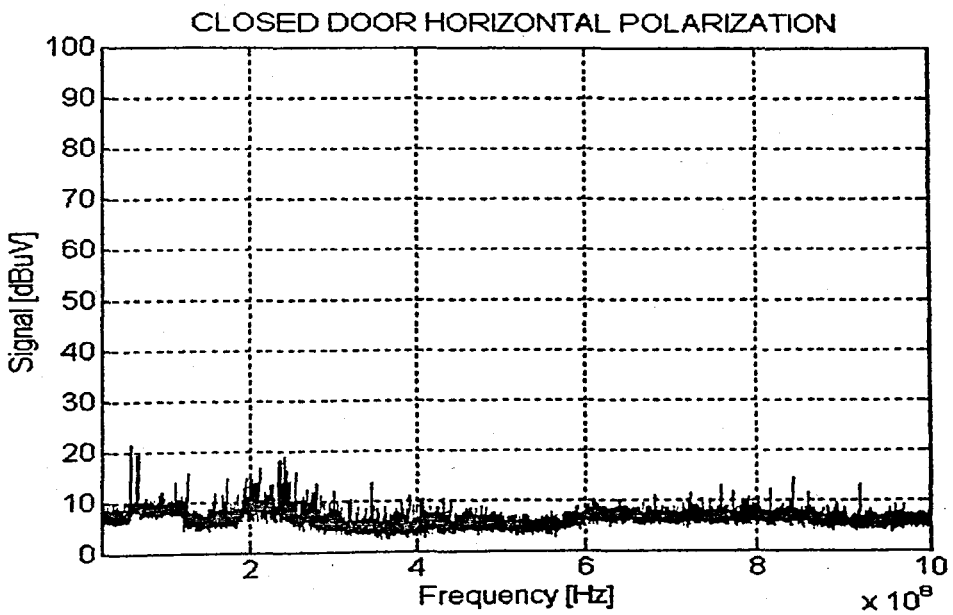

Figure 6.9. Before Absorbers Installation Closed Door Horizontal Polarization

Figure 6.8. and 6.9. show us the signal level inside CDC when the door is closed. Before the absorber material installation all signals could not be attenuated. Because of these signals at the resonance conditions some peak level can be observed in Figure 6.8 and 6.9. If we calculate the resonance frequencies of CDC from Eq.6.1. this equation yields frequency

values at the peak level of the Fig. 6.8 and 6.9. This is an important observation to understand the significant of the absorbers and the relations between the resonance frequency and the dimensions of the room.

Resonance frequency of a room is given as:[17]

$$f_r = 150\sqrt{\left(\frac{a}{l}\right)^2 + \left(\frac{b}{w}\right)^2 + \left(\frac{c}{h}\right)^2} \qquad (6.1)$$

where a,b,c=0,1,2... (but two of them is not equal to zero at the same time)
l, w, h is the length, width and the height of the room respectively. Therefore resonant frequency of CDC is calculated as

$$f_r = 150\sqrt{\left(\frac{1}{7}\right)^2 + \left(\frac{1}{3.04}\right)^2 + \left(\frac{1}{3.12}\right)^2} = 72.14\,MHz \qquad \text{for} \qquad a=b=c=1$$

Table 6.2. Resonance Frequency of CDC for Different Modes.

Resonance Frequency (MHz)	**a-b-c**
72.14	1-1-1
52.636	1-0-1
53.794	1-1-0
68.891	0-1-1
65.355	2-1-0
64.40	2-0-1
109.772	0-2-1
108.075	0-1-2
98.512	1-0-2
100.983	1-2-0
110.178	1-1-2
111.844	1-2-1
81.134	2-1-1
117.841	2-2-1
139.439	1-2-2
116.262	2-1-2
144.294	2-2-2

6.5.3. Measurement Results After Absorber Installation

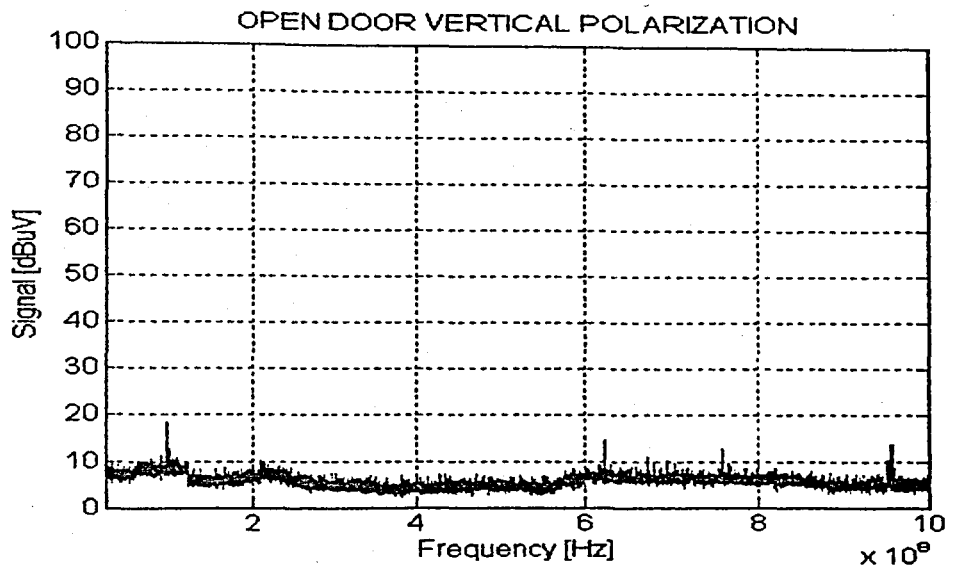

Figure 6.10. After Absorbers Installation Open Door Vertical Polarization

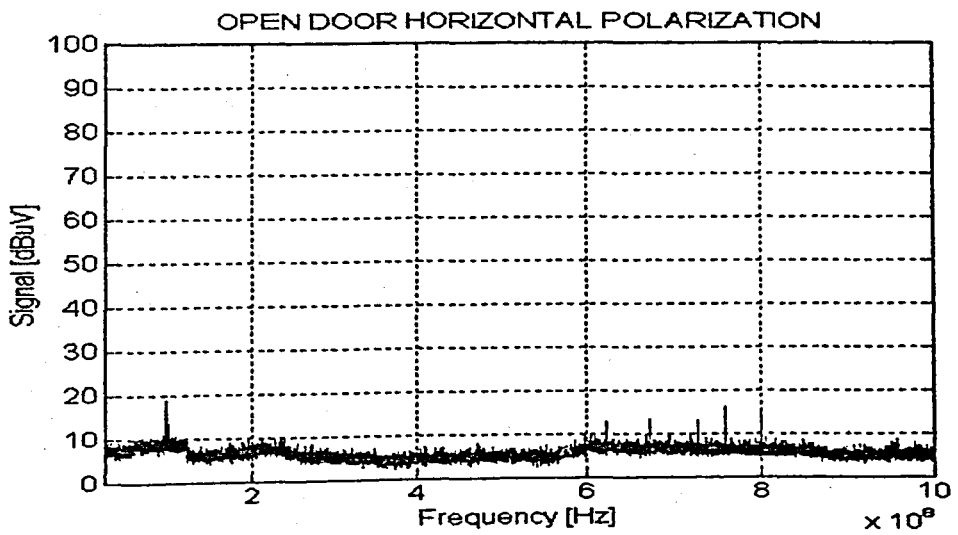

Figure 6.11. After Absorbers Installation Open Door Horizontal Polarization

After the absorber installation and the for open door case, signals were attenuated by the the wall more than the previous measurement. But there is still some peak level in the Figure 6.10 and 6.11. We can see from these figures, peak frequencies are diffremt for vertical and horizontal polarization. Because of the GSM has vertical polarization and broadcast TV stations have horizontal polarization only the dominant polarization can be seen in the figures.

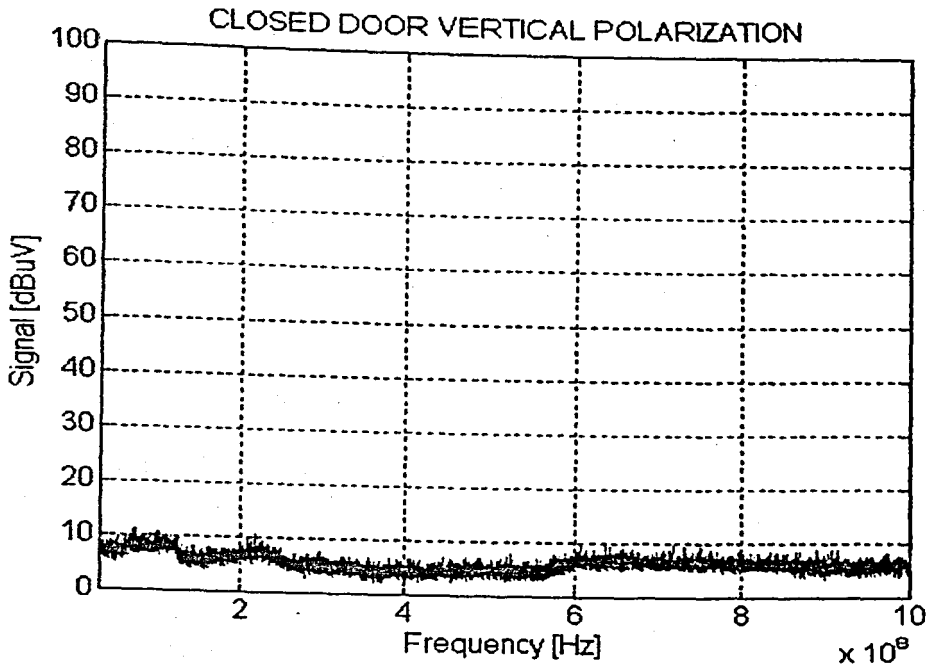

Figure 6.12. After Absorbers Installation Closed Door Vertical Polarization

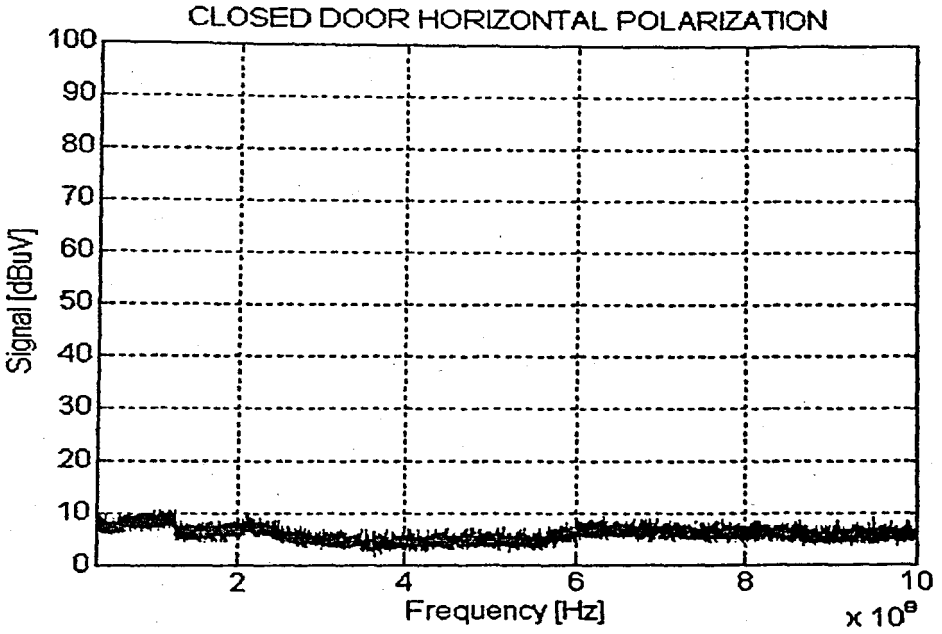

Figure 6.13. After Absorbers Installation Closed Door Horizontal Polarization

Finaly after the absorbers installation for the closed door case there is no signal inside the CDC

6.5.4. H Field SE Measurement of CDC

Magnetic field shielding effectiveness of the CDC was measured according to IEEE 299 Std. using the loop antennas as seen in the Figure 6.2.

Test Position 1-2-3-4-5-6: At the middle of the each side of the CDC door

Test Position 7-8-9 : Middle points of the seams

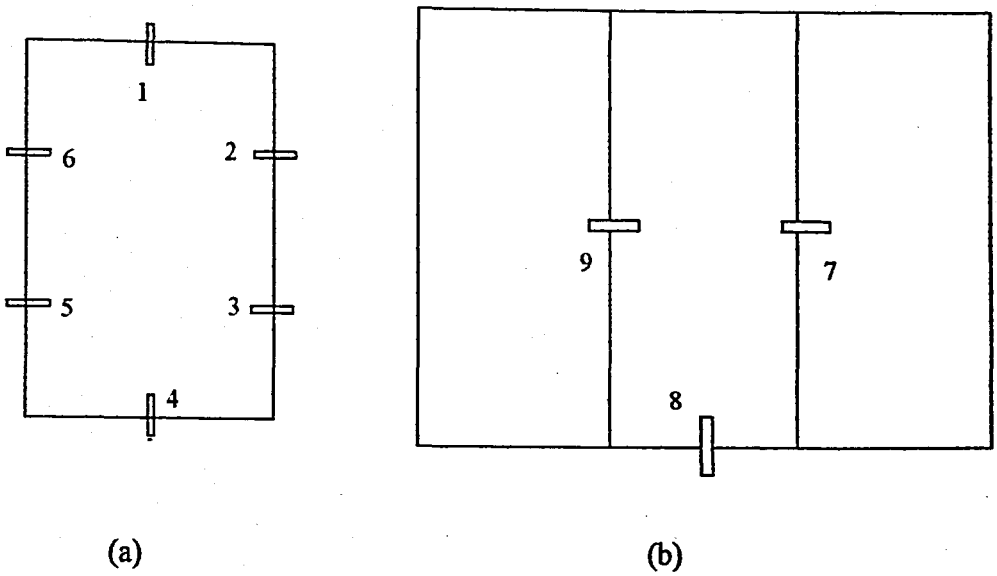

Figure 6.14. (a) Outside view of the CDC door
(b)Meassurement points of the CDC panel

Table 6.3. f= 10 kHz H Field SE of CDC
(CDC Noise Level 105 dB Ambient Noise Level: 100 dB)

Position	Horizontal(dB)	Vertical(dB)
1	105	100
2	90	100
3	95	98
4	100	90
5	100	100
6	95	102
7	96	98
8	100	100
9	105	103

Table 6.4.f=100kHz H Field SE of CDC
(CDC Noise Level 102 dB Ambient Noise Level: 98 dB)

Position	Horizontal (dB)	Vertical (dB)
1	110	107
2	108	105
3	100	100
4	100	98
5	97	100
6	105	102
7	110	105
8	100	100
9	105	103

Table 6.5. f=1MHz H Field SE of CDC
(CDC Noise Level: Max Ambient Noise Level: 115)

Position	Horizontal (dB)	Vertical(dB)
1	Max.	Max.
2	Max.	Max.
3	Max.	Max.
4	Max.	Max.
5	Max.	Max.
6	Max.	Max.
7	Max.	Max.
8	Max.	Max.
9	Max.	Max.

Table 6.6. f=10 MHz H Field SE of CDC
(CDC Noise Level: Max. Ambient Noise Level: Max)

Position	Horizontal (dB)	Vertical (dB)
1	Max.	Max.
2	Max.	Max.
3	Max.	Max.
4	Max.	Max.
5	Max.	Max.
6	Max.	Max.
7	Max.	Max.
8	Max.	Max.
9	Max.	Max.

6.5.5. H Field SE Measurement of GTEM

Magnetic Field SE measurements are made using the same measurements procedures of the IEEE 299 Std. At the test position given below.

Test Position 1: At the middle of the GTEM door

Test Position 2-3-4-5: Corners of the GTEM door

Test Position 6: Seams

Test Position 7: Camera (Honeycomb)

Test Position 8: Second door of the GTEM

Test Position 9: At the middle of the panel

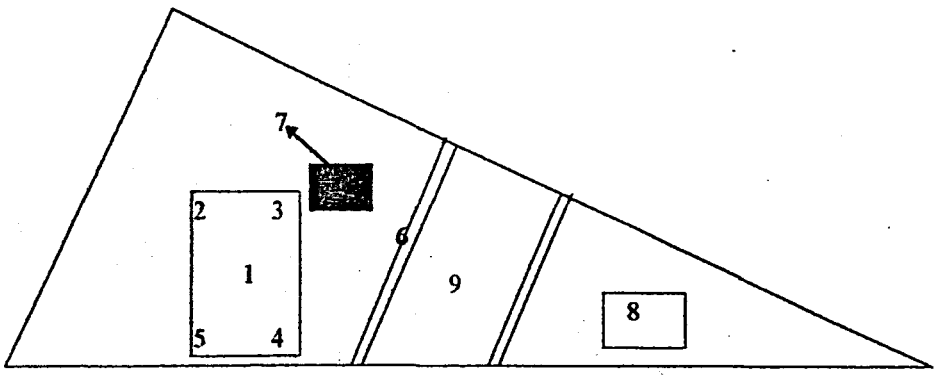

Figure 6.15. Measurement points of the GTEM

Table 6.7. f= 10 kHz H Field SE of GTEM
(GTEM Noise Level: 95-100 dB Ambient Noise: 95-100 dB)

Position	Horizontal(dB)	Vertical (dB)
1	55	55
2	45	46
3	45	40
4	55	50
5	60	50
6	45	62
7	39	47
8	53	53
9	53	53

Table 6.8. f= 100kHz H Field SE of GTEM
(GTEM Noise Level: 95-100 dB Ambient Noise: 95-100 dB)

Position	Horizontal (dB)	Vertical (dB)
1	66	64
2	58	61
3	58	46
4	65	70
5	70	70
6	60	78
7	46	60
8	48	48
9	67	68

Table 6.9. f= 1MHz H Field SE of GTEM
(GTEM Noise Level: 110 dB Ambient Noise: 120 dB)

Position	Horizontal (dB)	Vertical (dB)
1	87	84
2	75	77
3	76	63
4	82	86
5	89	90
6	79	98
7	65	67
8	67	67
9	86	86

Table 6.10 f=10 MHz H Field SE of GTEM
(GTEM Noise Level: Max. Ambient Noise:: Max.)

Position	Horizontal (dB)	Vertical (dB)
1	Max.	Max.
2	Max.	Max.
3	Max.	69
4	Max.	Max.
5	Max.	Max.
6	Max.	Max.
7	75	80
8	Max.	Max.
9	Max.	Max.

The results of the measurements show us CDC can attenuate the magnetic field than the GTEM. Because of the effective frequency range of the GTEM (30MHz-1GHz) this result was expected. However for both CDC and GTEM measurements SE values increase when frequency increases.

7. CONCLUSION

In this study a multilayer model has been selected to investigate the shielding properties of buildings. Shielding effectiveness of buildings and shielded enclosures were measured. The measurement site selected for this purpose was the building of the National Electronics and Cryptology Institute at the Marmara Research Center, TÜBİTAK.

The research has been carried out in two phases: In the first phase, a computer code simulating the multilayer model has been written in MATLAB. In order to asses the validity of the computer model, the code outputs have been compared with results of some previous research. Then it has been used to obtain the theoretical propagation loss of the walls in the building of our interest. The second phase has been entered by making attenuation measurements by an automated measurement system. The automation has been accomplished by the LAB Windows/CVI software via GPIB control. Two different situations have been tested. In the first one, the transmitting and the receiving antennas of the system have been located on the same floor of the building and the shielding effectiveness measurements have been carried out in the frequency range of 200 MHz -1000 MHz. In the second situation the receiver have been located one floor down and only one single frequency used during the measurements taken in various rooms (980 MHz).

The results of the measurements have been compared with the results obtained from the theoretical approach. We have seen that there is consistency especially for those frequency range where the clear space distance falls into the Fresnel region. But in general, the comparisons present more questions than answers as most of the frequency region could not fall into that region.

We have concluded that frequency scanning inside building is more complex than study at a single frequency. Since the clear space depends on the frequency and distance between transmitter and receiver measurements conditions always change during the scanning.

Multilayer model is an ideal case for building. Inside the building reflection and diffraction term should also be considered. We can see from the single floor modeling that reflection components decreased when the distance between transmitter and receiver increased.

Antenna directivity is another important point to be considered during measurements, since it is almost impossible to use an isotropic antenna in practice. If one uses directive antennas, alignment of the transmitting and receiving antennas must be maintained rigorously.

The measurements are supposed to be repeated in a recently constructed and unfurnitured building of TÜBİTAK. By repeating several similar measurements in a such empty building, it is expected to obtain measured results more consistent with the multilayer model studied in this research.

APPENDIX A

Typical Antenna Radiation Patterns of Conical Log Spiral Antenna

Radiation Pattern
Frequency: 300 MHz
Polarization Vertical

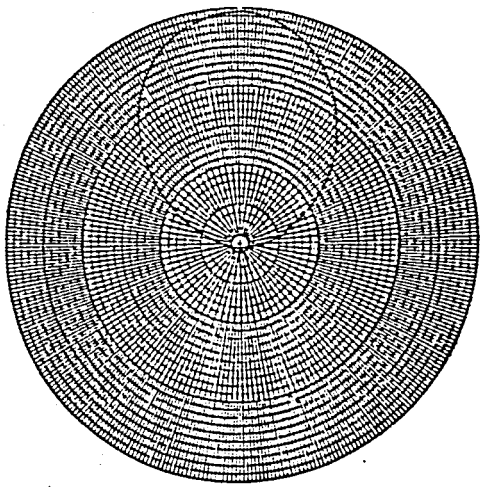

Radiation Pattern
Frequency: 300 MHz
Polarization Horizontal

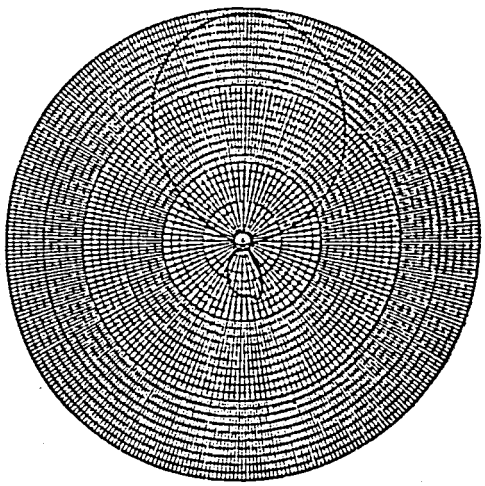

Radiation Pattern
Frequency: 500 MHz
Polarization Vertical

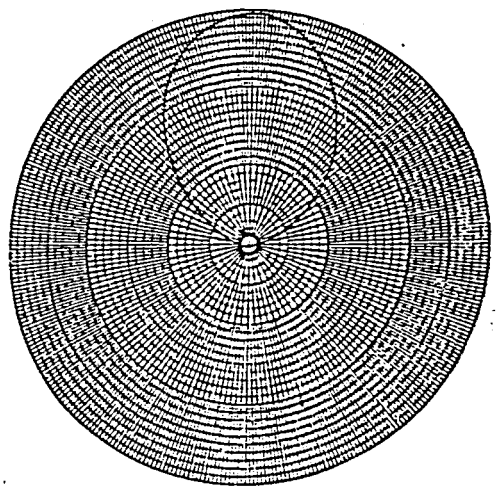

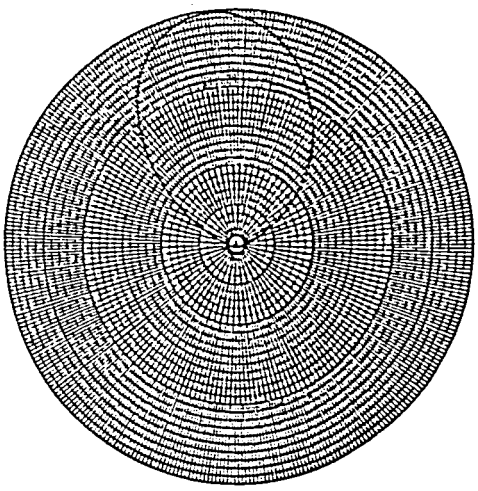

Radiation Pattern
Frequency: 500 MHz
Polarization Horizontal

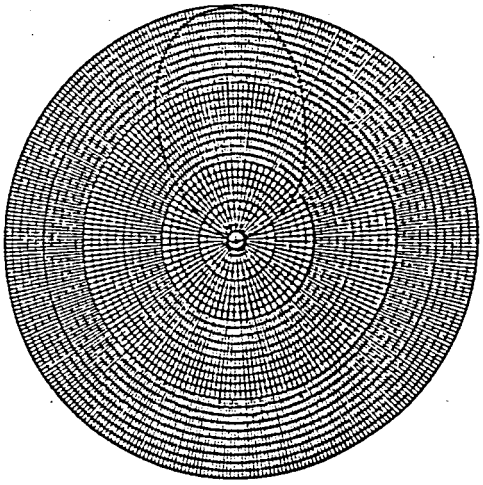

Radiation Pattern
Frequency: 900 MHz
Polarization Vertical

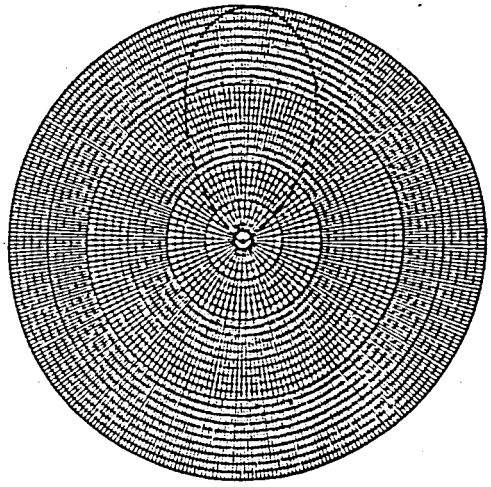

Radiation Pattern
Frequency: 900 MHz
Polarization Horizontal

REFERENCES

1. Alberta A. Smith, JR., "Attenuation of Electric and Magnetic Fields by Buildings," *IEEE Transaction on EMC*, Vol. EMC-20, No. 3, pp. 411-418, August 1978.
2. Jean-Francois Lafortune and Michel Lecours, "Measurement and Modeling of Propagation Losses in a Building at 900 MHz," *IEEE Transaction on Vehicular Technology*, Vol. 39, No. 2, pp. 101-108, May 1990.
3. Karahan O. " Electromagnetic Pulses, Their Characteristic and Effects on Random Layered Media," MS. Thesis, Boğaziçi University, 1988.
4. Demetrius T. Paris and F. Kenneth Hurd, *Basic Electromagnetic Theory*, McGraw-Hill, New York, 1969
5. Walter Honcharenko, Henry L. Bertoni, James L.Dailing, J Qian and H.D. Yee, "Mechanism Governing UHF Propagation on Single Floors in Modern Office Buildings," *IEEE Transactions on Vehicular Technology*, Vol. 41, No. 4, pp. 496-504 November, 1992.
6. Walter Honcharenko, Henry L. Bertoni, James L.Dailing, "Mechanism Governing Propagation Between Different Floors in Buildings" *IEEE Transactions on Antenna and Propagation*, Vol. 41, No. 6, pp. 787-790 June 1993
7. Donald R. J. White, *A Handbook Series on Electromagnetic Interference and Compatibility Volume 3 EMI Control Methods and Techniques*, Interference Control Technologies, Inc., Virginia, 1986
8. Donald R. J. White, *A Handbook Series on Electromagnetic Interference and Compatibility Volume 3 Electromagnetic Shielding*, Interference Control Technologies, Inc., Virginia, 1988
9. Donald R. J. White, *A Handbook Series on Electromagnetic Shielding Materials and Performance*, Interference Control Technologies, Inc., Virginia, 1988
10. Paul I. Wells, "The Attenuation of UHF Radio Signals by Houses," *IEEE Transaction on Vehicular Technology*, Vol. VT-26, No.4, pp.358-362, November 1977.
11. S. S. Şeker and N. Ari, Analysis of Broad Band Absorbing Materials Using Multilayer Structures, ABB Ref. No:PE-04,1986

12. Demetrius T. Paris, "Computer-Aided Radom Analysis," *IEEE Transactions on Antennas and Propagation*, Vol. AP-18, N0.1, pp. 7-15, January 1970.

13. DOD USA, *Military Standard Attenuation Measurements for Enclosures, Electromagnetic Shielding, for Electronic Test Purposes, Method of*, United States Government Printing Office, Washington, 1956.

14. ANSI *IEEE Standard Method for Measuring the Effectiveness of Electromagnetic Shielding Enclosures* , The Institute of Electrical and Electronics Engineers, Inc., New York, 1991

15. Edwin L. Bronaugh, "IEEE Std 299-1991: New Shielding Effectiveness Measurement Standard", *EMC Test &Design*, pp 43-46, February 1993.

16. T. Howe, "Automated Testing of Shielding Effectiveness," *ITEM*, pp.215-220, 1992.

17. Selim Şeker and Osman Çerezci, *Electromagnetik Dalgalar ve Mühendislik Uygulamaları*, Boğaziçi Üniversitesi, İstanbul, 1994

REFERENCES NOT CITED

Keenan and A.J. Moltey, "Radio Coverage in Buildings," *British Telecom Technology J.*, Vol. 8, No. 1, pp.19-24, January 1990.

Hamilton W. Arnold, R.R. Murray and Donald C. Cox, "815 MHz Radio Attenuation Measured Within Two Commercial Buildings," *IEEE Transactions on Antenna and Propagation*, Vol. 37, No. 10, pp. 1335-1339, October 1989.

Constantine A. Balanis, *Antenna Theory Analysis and Design*, Jonh Wiley&Sons, New York 1982

Alfonso Aiello, Marco Righetti, Giovanni Tribellini, "A Theoretical Model for Thin Shield Effectiveness of Rectangular Cases," *EMC 96 International Wroclaw Symposium on Electromagnetic Compatibility*, pp 540-544, June 1996

Walter Honcharenko and Henry L. Bertoni, "Transmission and Reflection Characteristics at Concrete Block Walls in the UHF Bands Proposed for Future PCS," *IEEE Transaction on Antenna and Propagation*, Vol. 42, No. 2, pp.232-239, February 1994.

Molkdar, "Review on Radio Propagation into and within Buildings," *IEE Proceedings-II*, Vol.138, No.1, pp. 61-73, February 1991.

Haim Cory, Shabtay Shiran and Monica Heilper, "An Iterative Method for Calculating the Shielding Effectiveness and Light Transmittance of Multilayered Media," *IEEE Transaction on EMC*, Vol.35, No. 4, pp.451-456, November 1993.

A. J. Mauriello, "Development of a Doorless Access Corridor for Shielded Facilities," *IEEE Transaction on EMC*, Vol. 31, No.3, pp. 223-229, August 1989.

Homayoun Hashemi, "The Indoor Radio Propagation Channel," *Proceedings of the IEEE*, Vol. 81, No.7, pp. 943-968, July 1993.

Gerald M. Whitman, Kyu-Sung Kim and Edip Niver, "A Theoretical Model for Radio Signal Attenuation Inside Buildings," *IEEE Transaction on Vehicular Technology*, Vol. 44, No. 3, pp.621-629, August 1995.